

## CHAPTER 2

---

### LARGE AMPLITUDE OSCILLATIONS IN A PARABOLIC TROUGH

#### NARRATIVE - CONNECTION TO THE TEXT

Chapter 2, Sec.13.2 describes oscillatory fluid motion within a parabolic cross section trough. There are several analytical solutions to the depth averaged equations of motion and continuity under these conditions. This offers a useful comparison with NLSW model results. Various runup / rundown algorithms and sea level reconstructions can be tested under large amplitude wave conditions. Two full cycles of the two lowest modes oscillation are animated here – accompanied with an assessment of model errors accumulated over a span of 5 cycles

#### MODEL DESCRIPTION

- The animations below depict motion of the two lowest “slosh” modes. Dimensions of the trough are as described by Eqn. (2.123) in the text and shown in Figure-movie 2.1.
- A 1-D, non-linear shallow water wave model is used to solve numerically for  $u(x, t)$  and  $\zeta(x, t)$ . To be consistent with the analytic results however, bottom friction is dropped.
- Spatial step size  $\Delta x$  is 100 m, time step is .005 s.
- Position along the  $x$  axis is denoted by  $x = \Delta x * i$  where  $i = 1, 2, 3, 4, \dots, 1601$
- Animation frames were generated at 25 s intervals to depict two full periods of oscillation ( $\tau = 1998$  s for the lowest mode, and  $\sim 1152$  s for the next higher mode)
- The initial conditions for the two animations are:
  - Mode 1:  $U(x, 0) = 0, \zeta(x, 0) = .01 * x$
  - Mode 2:  $\zeta(x, 0) = 0, U(x, 0) = 6.34 \times 10^{-4} s^{-1} * x,$
- Equations of motion and continuity are modeled with Eqns. (2.121) and (2.122) respectively as displayed in the text. Flux formulations for sea level updates (Eqn. 2.102) are used to insure conservation of mass.
- The runup algorithm is shown in Fig. 2.32 of the text and the rundown algorithm is shown in the Fortran code “snippet” preceding the figure

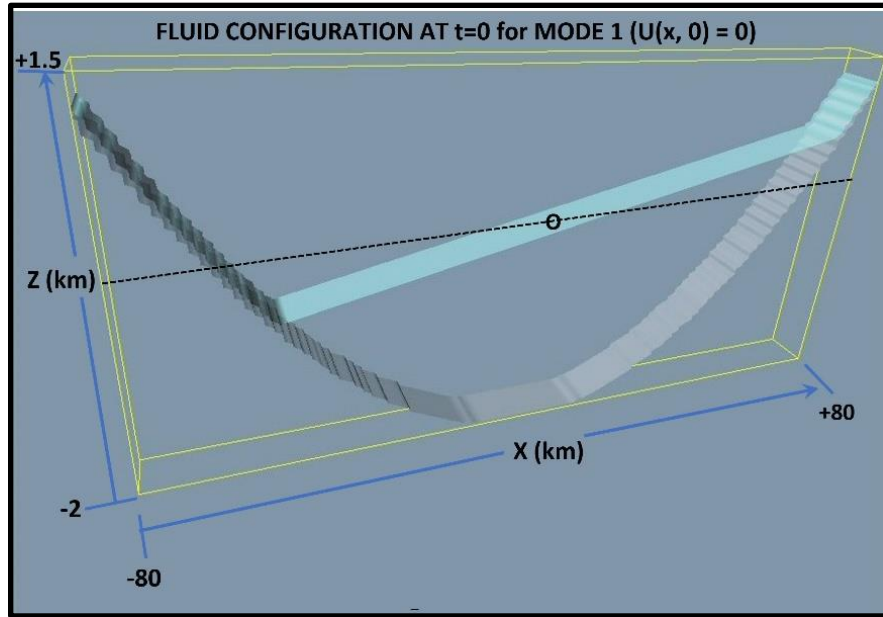


Figure-movie 2.1 - model domain with mode 1 initial conditions

[<CLICK HERE TO WATCH THACKER\\_1.MP4>](#)

[<CLICK HERE TO WATCH THACKER\\_2.MP4>](#)

## MODEL SUMMARY

Sea level dynamics and oscillation periods for both modes track closely with analytic expectations (Figure-movie 2.2 below). The period of oscillation for mode 1 is 1998 s and is identical to numerical results even after 5 cycles of motion. The maximum modeled sea level slope drops by .06 % during this same time. This is expected as the numerical system slowly “runs down”.

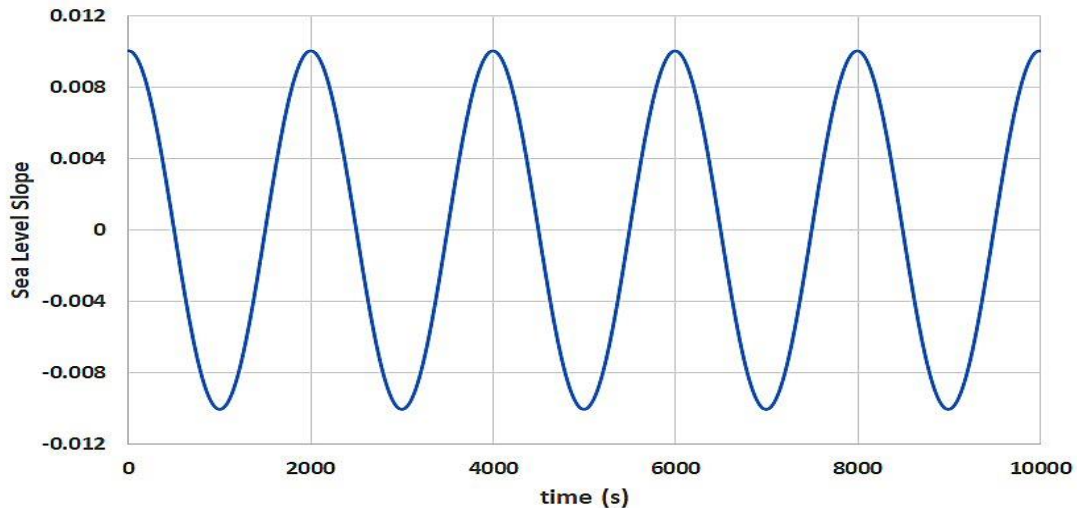


Figure-movie 2.2 - sea level slope - Mode 1

Accumulated errors in the mode 2 model for system energy and mass are plotted below in Figure-movie 2.3

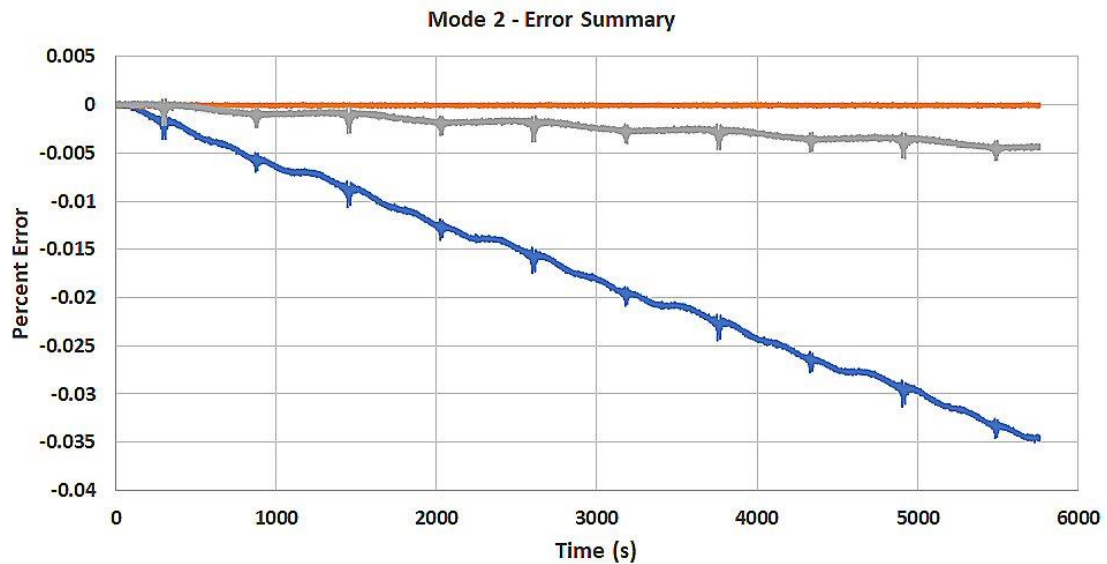


Figure-movie 2.3 Red curve: mass error, blue curve: total system energy error using piecewise constant sea level reconstruction, gray: total system energy with piecewise linear sea level reconstruction

Mass is conserved throughout the 5 cycles of oscillation. Energy (kinetic + potential) is slowly lost however. The error spikes occur at moments of maximum runup and minimum rundown.

## DAM-BREAK PROBLEM

### NARRATIVE - CONNECTION TO THE TEXT

The dam-break problem is one of the oldest hydraulic problem whose solution derived by the method of characteristics is given below in the left panel. The dam breaks instantaneously at  $t=0$  and generates two waves: a negative wave propagating into the fluid and a positive wave propagating over the dry bed. The wave front of the non-viscous fluid propagates over the dry-bed with speed  $2\sqrt{gD_0}$  which is two times greater than the wave front speed moving in the negative direction. At the dam site, the water depth drops instantaneously to a constant value of  $\frac{4}{9}D_0$ , where  $D_0$  is the initial depth, (Figure-movie 2.4 left panel).

In the right panel the analytical solutions (continuous lines) and numerical solution have been compared. Although results are quite good, a magnified picture of the free wave profile shows that the numerical solution profiles lag slightly behind the analytical profile. The computations presented in the right panel are elucidated in Chapter 2. They are based on the finite-difference approach and a special algorithm for the runup.

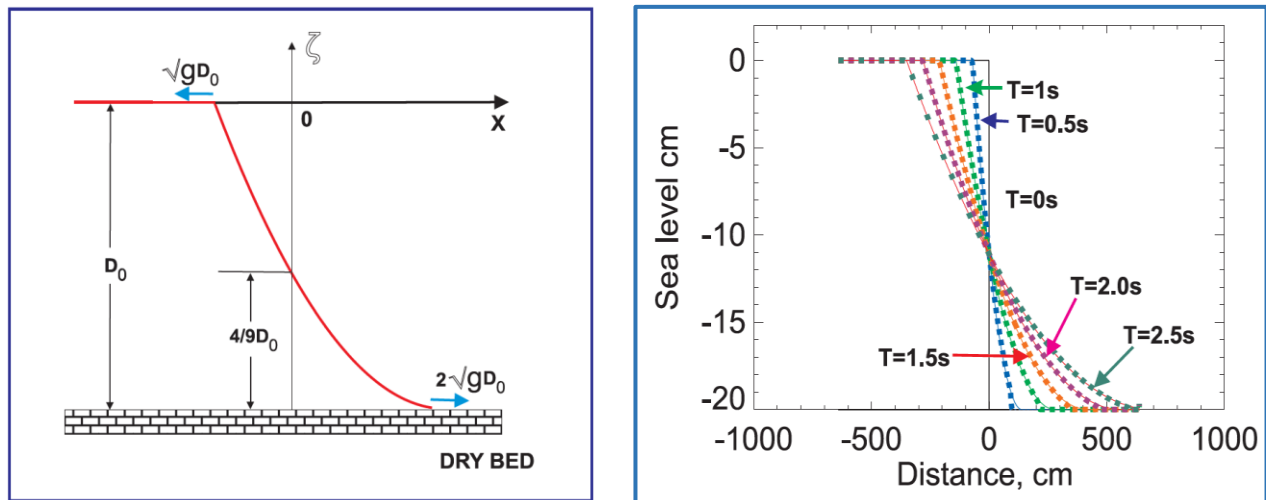


Figure-movie 2.4 – Dam break problem: left panel analytical solution, right panel numerical solution.

Below we present two movies which results from the dam-breaking solution by the FNS-VOF Model, which is Full Navier-Stokes equation aided by the Volume of Fluid method. (See Chapter 6, Sec. 6.2.3). This method solves for two-dimensional fluid flow with tracking of the free surface. The free surface of the fluid is described by the

discrete VOF function; this approach was conceived way back by Nichols and Hirt (1975).

## MODEL DESCRIPTION

- The animations below describe the dam break problem using NVS-VOF model and compares its solution with analytical (Figure-movie 2.5) and lab experiment (Figure-movie 2.6)
- The NVS-VOF 2-D model solves vertical and horizontal motion. Velocities  $u$ ,  $w$  are solved by the two step methods for the solution of the pressure field. The free surface is determined based on the VOF function which is defined by the fraction of fluid in the computational cells.
- Spatial step along the horizontal and vertical is 0.0025 m and time step is  $2.0e-4$  s.
- Density is  $1000 \text{ kg/m}^3$  and the dam height is  $h_0 = 2.0\text{m}$ , for Figure-movie 2.5 and  $h_0 = 0.2\text{m}$ , for Figure-movie 2.6. The motion of the gate in the Figure-movie 2.5 is instantaneous and in the NVS-VOF vs lab experiment is given by  $z(t) = 23.6t^2 + 0.134t$  where  $t$  is time in s.
- The initial conditions for the dam break problem are:
  - Figure-movie 2.5,  $u(x, y) = 0$ ,  $w(x, y) = 0$  and  $h_0(-10 < x < 0\text{m}) = 2.0\text{m}$
  - Figure-movie 2.6,  $u(x, y) = 0$ ,  $w(x, y) = 0$  and  $h_0(-7.5 < x < 0\text{m}) = 0.2\text{m}$
- Equations of continuity and motion are modeled with Eqns. (6.10) and (6.11) respectively. The free surface of the dam break fluid is modeled by the discrete VOF scheme, Eqn (6.16) and the  $F(\vec{x}, t)$  function.

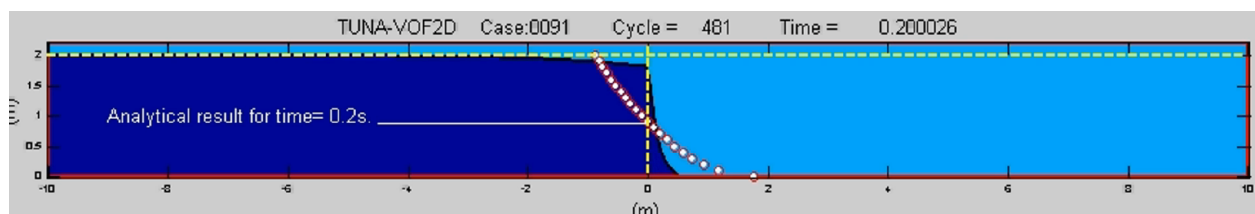


Figure-movie 2.5 NVS-VOF numerical solution versus analytical solution.

[CLICK HERE TO WATCH CASE 0091.MP4](#)

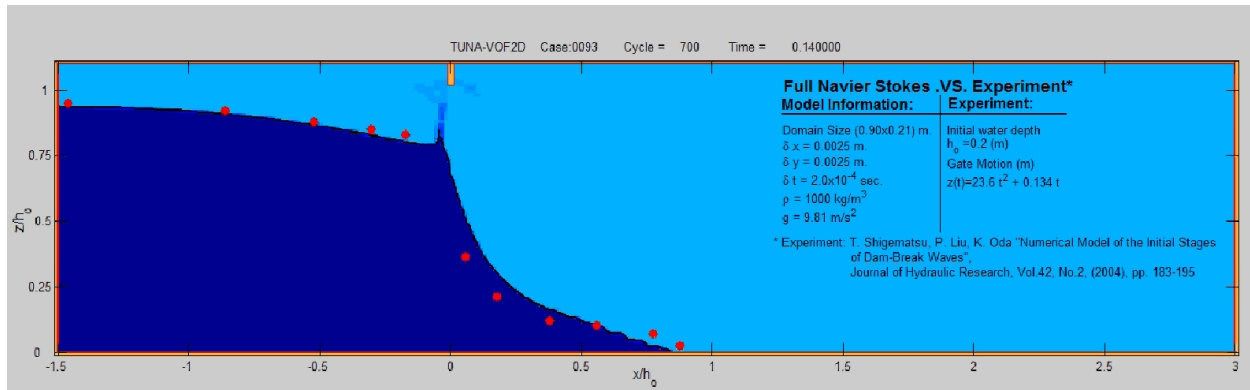


Figure-movie 2.6 NVS-VOF numerical solution versus lab experiment, Shigematsu et al., 2004.

[<CLICK HERE TO WATCH CASE\\_0093.MP4>](#)

## MODEL SUMMARY

From above experiments it is evident that initial phase expressed by the analytical solution is not well reproduced (which is expected), however as time progresses, better agreement is observed. It is also noticed that in the lab experiment the effect of the gate motion plays an important role at the initial phase and model result gets better agreement as time advances. The speed of removing the gate may also play an important role.

## CHAPTER 3

### REVERSE FAULT SOURCE AND INITIAL COASTAL RECESSION VS INUNDATION

#### NARRATIVE - CONNECTION TO THE TEXT

For the Indian Ocean tsunami, first wave arrivals at coastal points east of the source tended to be troughs, while those to the west were crests. The ocean bottom deformations used as sources for both the IOT and the KIT show a similar pattern of uplift and down drop (Figure 3.9 from textbook for the IOT source deformation contours). Representing the initial wave as a “copy” of the bottom deformation as indicated in Figure-movie 3.1, and then expressing this as a sum of right and left traveling wave as in Chapter 2, Eqn. (2.7) offers an explanation of the signs of these first wave motions at coastal points.

#### MODEL DESCRIPTION

- The animation depicts the effect of a simplified “dipolar” earthquake source which includes both down drop and uplift within the fault zone. This is commonly seen with reverse or thrust fault mechanisms as tsunami sources. The resulting wave dynamics show how coastal points at opposite sides of a fault can record opposite senses of “first wave motion”.
- This is a 1D, transient shallow water wave model  $u(x, t)$  and  $\zeta(x, t)$  – with no non-linear terms. Depth is uniform at 1000 m.
- Spatial step size  $\Delta x$  is 1 km, time step is 1 s.
- The position along the  $x$  axis is denoted by  $x = \Delta x * i$  where  $i = 1, 2, 3, 4, \dots, 1000$
- The earthquake source is confined to  $400\text{km} < x < 600\text{km}$ , with uplift rise time ( $t_{max}$ ) of 10 s, width ( $\lambda$ ) = 200 km (centered at  $x_0 = 500$  km), and maximum uplift ( $\eta_0$ ) of 2 m. The source is modeled as  $n = \eta_0 \frac{t}{t_{max}} \text{SIN}\left\{\frac{2\pi(x-x_0)}{\lambda}\right\}$  for  $0 < t < t_{max}$ .
- 180 animation frames were generated at 25 s intervals - giving 1.25 hours of wave evolution. The animation rate is slowed by 25X during uplift ( $0 < t < t_{max}$ ) so the viewer can visualize the otherwise near-instantaneous source in action.

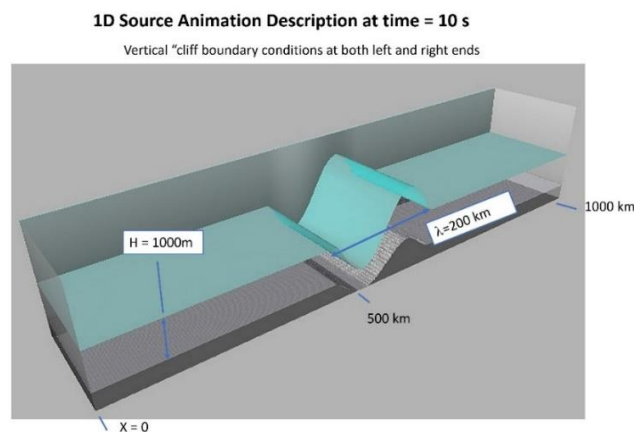


Figure-movie 3.1 1D source animation with left and right traveling waves.

[<CLICK HERE TO WATCH MOVIE \(ReverseFaultSource.mp4\)>](#)

## MODEL SUMMARY

Sea level at three times (Figure-movie 3.2): *blue* at  $t_{max}$  (10s), *red* at 2500s, and *grey* at 4800s. Note the opposite polarities of the wave arrivals at  $x = 0$ , and 1000 km at  $t=4800$ s. The lack of spread or drop in amplitude of the initial sea-level deformation (blue curve) shows that the uplift can be treated in this case as nearly instantaneous.

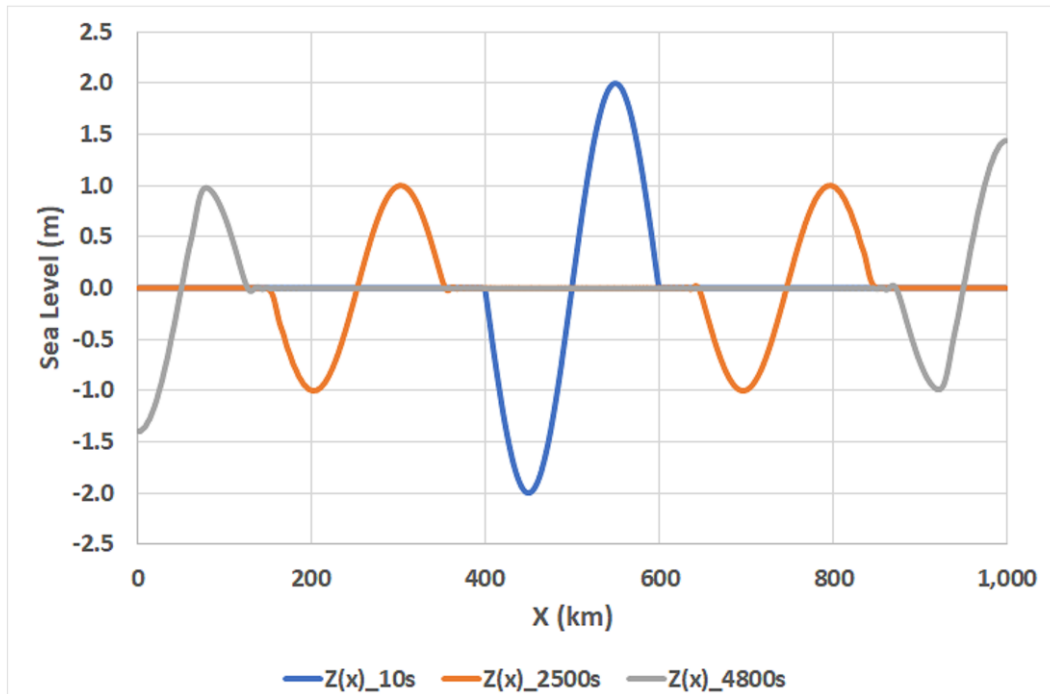


Figure-movie 3.2 1D source snapshots of wave approaching left and right coasts. Blue, initial wave; red, open ocean and gray, wave arriving coasts.

## ST. AUGUSTINE VOLCANO SOURCE, GENERATION AND MAXIMUM WAVE AMPLITUDE IN COOK INLET

### NARRATIVE - CONNECTION TO THE TEXT

The simulation of tsunami caused by landslide, presented in Chapter 3.14, is further explained by considering the eruption of the Mount St. Augustine volcano in 1883. During the eruption, a portion of the volcano collapsed into the shallow water of Cook Inlet (Kienle et al., 1987).

### MODEL DESCRIPTION

A numerical model was used to calculate the tsunami generated by the debris flow from the volcano's collapse. The source of debris is located on the volcano's eastern side, and Figure-Movie 3.3 provides the basic parameters of the slide.

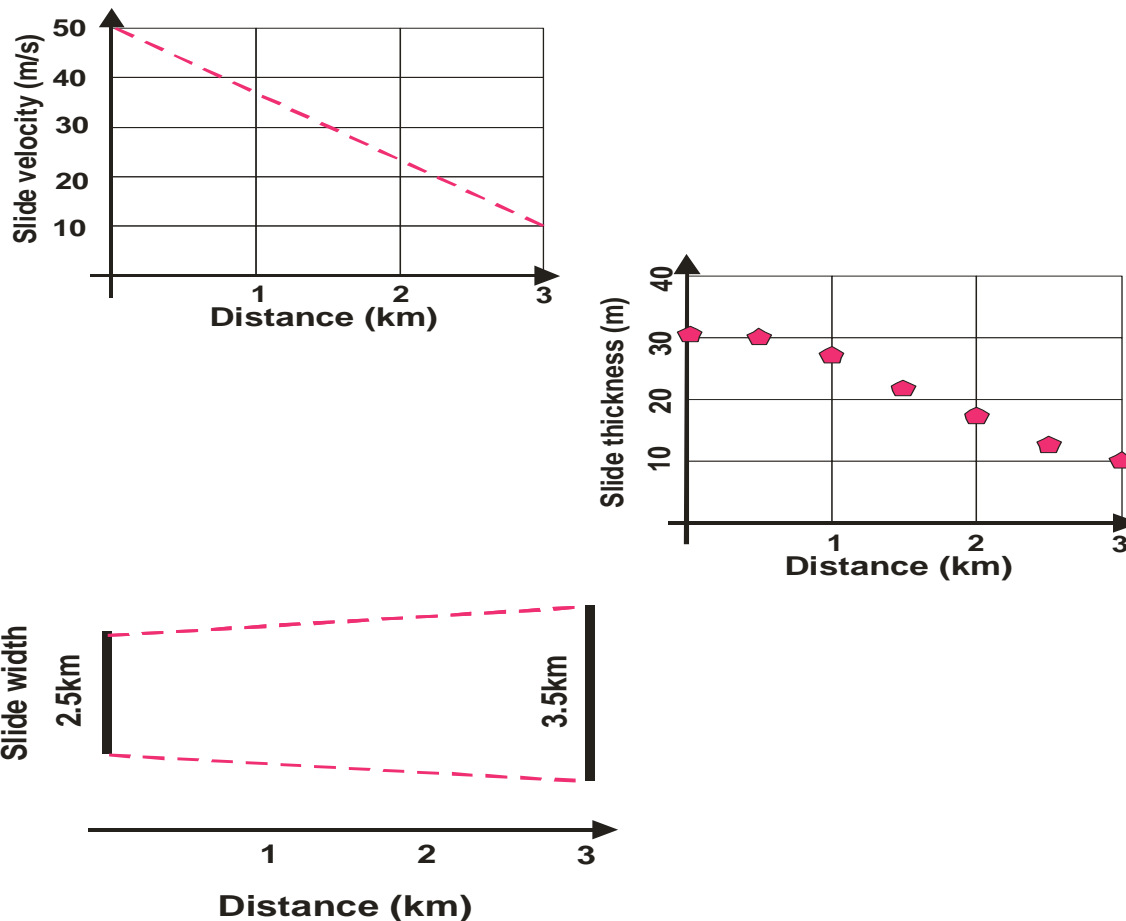


*Figure-movie 3.3. Slide velocity, thickness and width as a function of the distance for the eastern St. Augustine slide.*

The distance of 3km in this figure describes the travel distance of the slide from the time it entered Cook Inlet water. Along this distance, the travel velocity of the slide diminished from 50 m/s to 10m/s, its thickness along the center of the slide also diminished from 30m to 10m, while the slide width increased

approximately from 2.5km to 3.5km. This debris flow was simulated as a progressive flow of the bottom uplift, which imparted motion to the water column.

The tsunami's generation and propagation are calculated using a set of equations of motion and continuity for the long wave equations. The numerical form of these equations and appropriate boundary conditions for the land/water and water/water boundaries are given in Chapter 4. The finite-difference equations are solved in the spherical system of coordinates with the grid spacing of 1 minute along the E-W direction and 0.5 minutes along the N-S direction. The Cook Inlet domain depicted in Figure-movie 3.4 spans from 58 50'N to 61 50'N and from 154 18'W to 148 18'W.

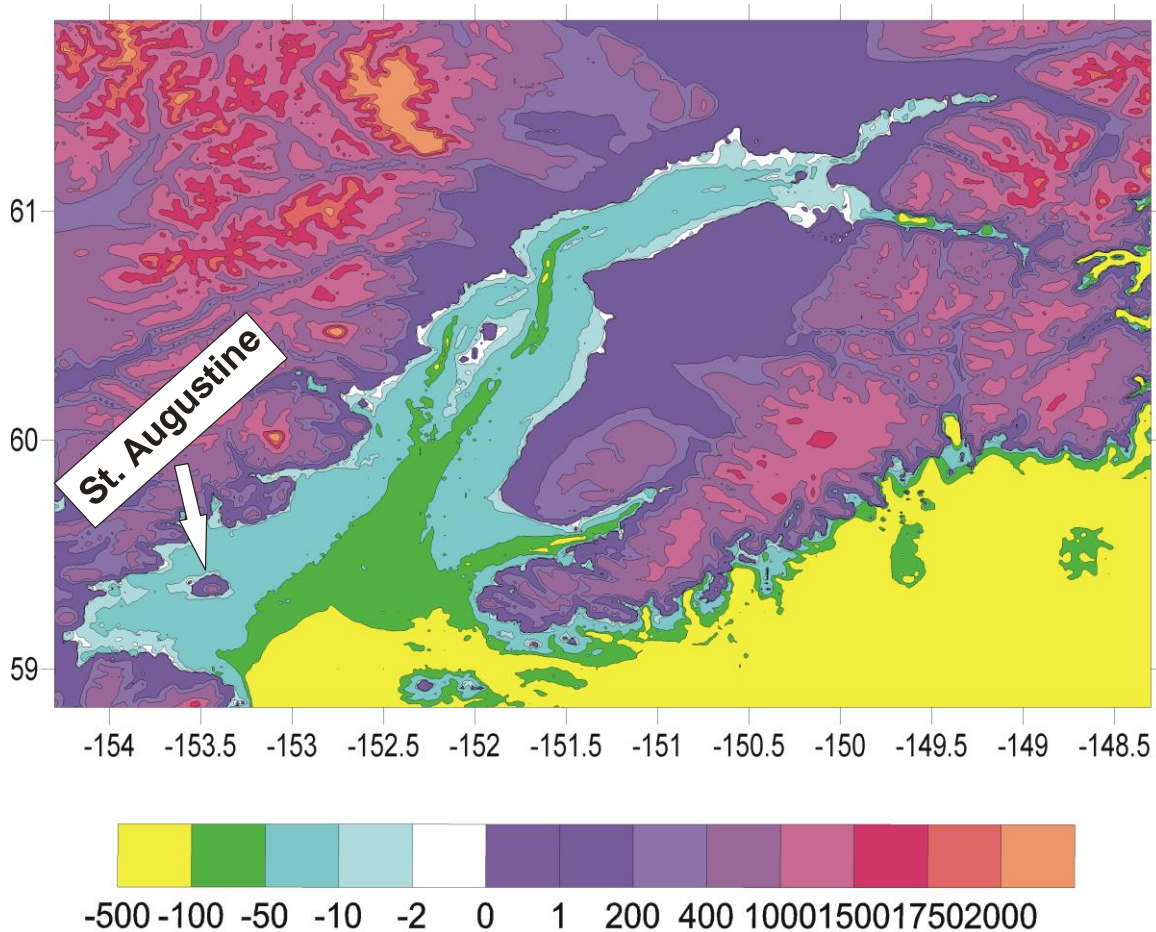
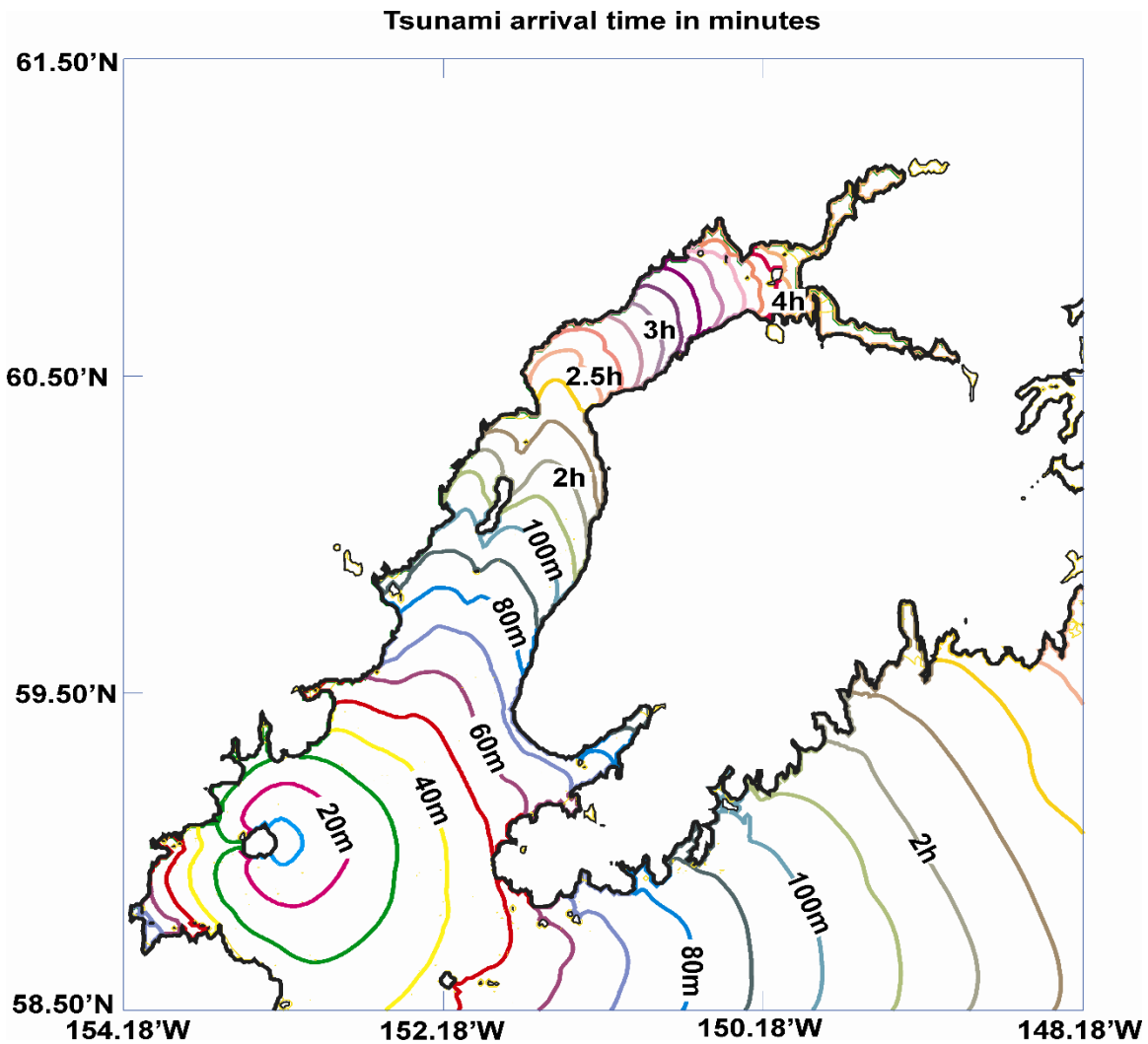


Figure-movie 3.4. Bathymetry (negative) and relief (positive) of the Cook Inlet domain used in numerical computations. Numbers are in meters.

The first result of numerical computation given in Figure-movie 3.5 defines travel times to various locations. Tsunami travel time to Homer is close to 75min, while travel time to Anchorage is around 4 hours.



*Figure-movie 3.5. Tsunami arrival time for the eastern slide.*

Figure-movie 3.6 describes the contours of the maximum tsunami amplitude. This is the greatest wave height during the 5 hours of the process. Usually, the maximum amplitude occurs at the different grid points at different times. The spatial distribution of the maximum amplitude defines the directional properties of the tsunami source; therefore, the maximum in Figure 3.6 is directed eastward, away from St. Augustine. While propagating towards the shorelines, the tsunami amplitude is amplified along the peninsulas and ridges. Westward from St. Augustine in the shallow waters of Kamishak Bay, tsunami amplitude is dissipated through the bottom friction.

## TSUNAMI MAXIMUM AMPLITUDE

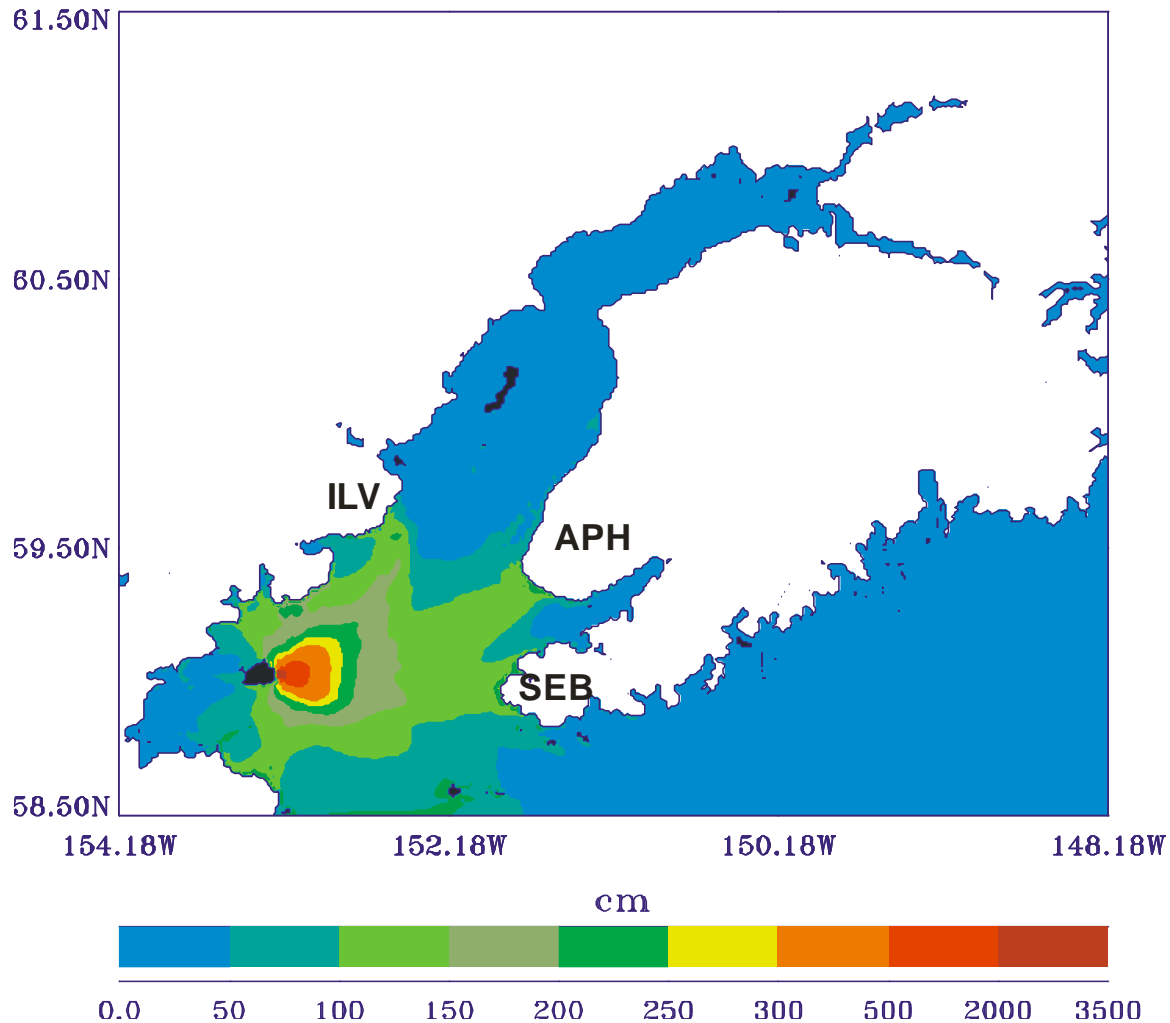


Figure-movie 3.6. Maximum tsunami amplitudes in centimeters. Abbreviations: APH, Anchor Point -Homer; SEB Seldovia-English Bay; ILV, Iliamna Volcano.

The strongest amplification occurred along the Seldovia-English Bay shoreline, up to approximately 2.5m (Figure-movie 3.6). Amplitudes of about 2m occur along Anchor Point -Homer (APH) shoreline and along Iliamna Volcano (ILV) shoreline. This amplification is essential for the coastal communities along the eastern shore of Lower Cook Inlet as the tsunami travels to SEB in 50 min and to APH in about 75 min; therefore, warning time for these communities is relatively short.

We have produced two movies to describe better the above results. The movie titled Maximum amplitude (Figure-movie 3.7) checks the amplitude in every grid point while the signal propagates from the source, and only the maximum wave height is retained. The final distribution of the maximum wave height is also plotted in Figure-movie 3.6.

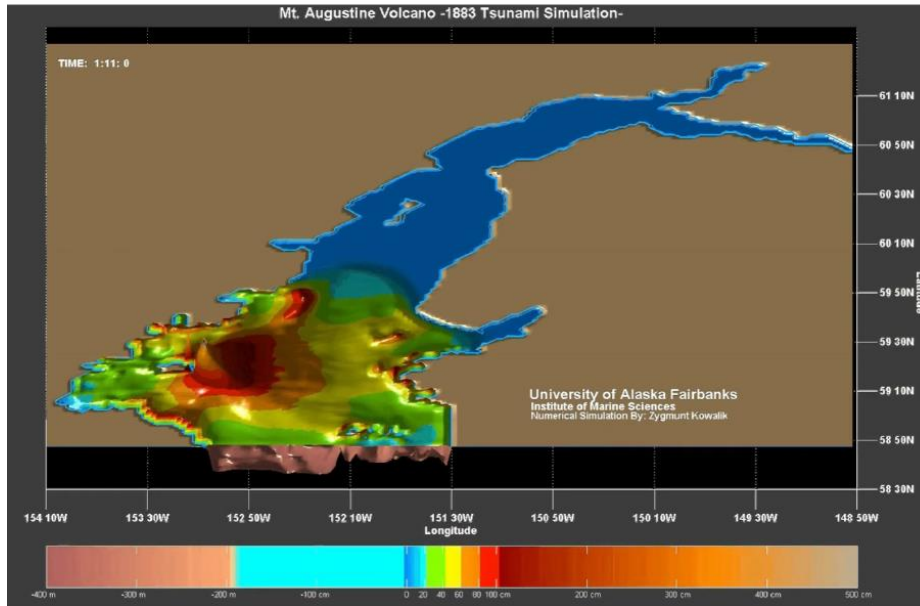


Figure-movie 3.7 Maximum wave amplitude recorded in time due to the flank collapse of the St Augustine volcano.

[<CLICK HERE TO WATCH MOVIE \(Maximum Amplitude.mp4\)>](#)

The propagation in time of the tsunami signal is given below (Figure-movie3.8) in the movie titled amplitude in time. Out of this movie, the tsunami arrival time is calculated and plotted in Figure-movie 3.5.

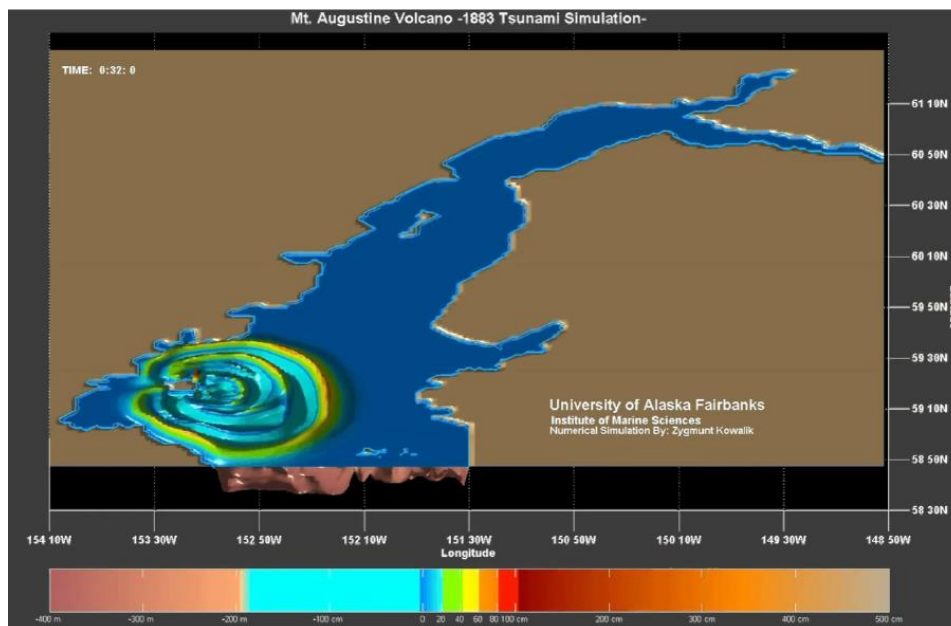


Figure-movie 3.8 Tsunami wave propagation in time due to the volcano flank collapse of the St Augustine volcano

[<CLICK HERE TO WATCH MOVIE \(amplitude in time.mp4\)>](#)

## **MODEL SUMMARY**

Numerical computation shows travel time and maximum amplitude as important parameters for hazard mitigation in the coastal communities. Computations delineate the important role of bathymetry in tsunami coastal amplification where submerged peninsulas or ridges serve as tsunami guides.

### References:

Kienle, J., Z. Kowalik, and T. Murty. 1987. Tsunami generated by eruption from Mt. St. Augustine volcano, Alaska. *Science* 236:1442-

## CHAPTER 4

---

### GLOBAL TSUNAMI PROPAGATION

#### NARRATIVE - CONNECTION TO THE TEXT

Chapter 4 presents numerical tools for the investigation of tsunami propagation in the World Ocean based through modeling the Indian Ocean Tsunami (IOT) of December 2004, the Kurile Island Tsunami (KIT) of November 2006 and the Japan Tsunami (JT) of March 2011.

#### MODEL DESCRIPTION:

The global model for the IOT, 2004 was formulated in spherical polar coordinates. Grid points were assigned to the World Ocean from 80 south latitude to 69 north latitude with a spatial resolution of one minute. This resulted in a massive 220 million grid points. Using Whitmore's source function that showed the sea floor's tectonic activity and the subsequent vertical displacement of water. Energy flux was implemented to investigate energy transfer from the tsunami source across the India Ocean to the Atlantic and Pacific Oceans. The sheer size of the computational domain of the global model required a parallel code. The entire domain was split along meridians into 40 subdomains and was run on a supercomputer, Cray X1 (Arctic Research Supercomputer Center, University of Alaska, Fairbanks). The computational task took less than 10 hours on 60 multi-streaming processors, just under half the machine maximum capability.

The Kurile Island Tsunami, 2006 model was also formulated with one minute grid spatial resolution (7800x2640 grid points). The source function is given in Figure 4.22. The tsunami spreads along the entire Ocean Pacific, but the main tsunami signal was confined in the northern hemisphere. Several important bathymetric features (Guyot inset), and scattering dynamics (energy flux) are discussed further to understand the Kurile Tsunami transformation.

#### MODEL SUMMARY

##### INDIAN OCEAN TSUNAMI, 2004

The movie below depicts propagation of tsunami only in the Indian Ocean in December 2004 while looking from above at the ocean surface. The source function, i.e. the bottom uplift has been described in **Chapter 3, Sec.4**. The movie (Figure-movie 4.1) is strictly related to the **Chapter 4, Sec.3**. The movie shows wave propagation in real time. Initial bottom uplift generates two wave-systems, one traveling to the East into Indonesian Islands and the second wave propagates to the West towards India and Maldives Island. The wave moving to the India and Sri Lanka is strongly reflected from Sri Lanka sending tsunami towards South-East. The reflected wave from the Bay of Bengal again is directed towards south, thus this signal will combine with Sri Lanka signal and travel along deep ocean ridges towards Antarctica. The wave front directed towards Maldives Islands is transformed into three different signals: the reflected waves which join signals from Sri Lanka and Bay of Bengal. The trapped signal which stays around Islands and the passing

signal which continues its travel towards Arabian Peninsula, Africa and Atlantic Ocean. It is interesting to notice that the wave front blocked by Maldives converges behind the Islands resulting in the focusing tsunami energy by this long island chain (see wave front west of the Maldives). One of this secondary energy beams directed towards the coast of East Africa caused sea level rise to 3.3 meters. Both computations and observations demonstrate a significant increase of the tsunami amplitude of up to 1.5 m at the coast of Arabian Peninsula. The movie was produced at the Arctic Research Supercomputer Center of University of Alaska, Fairbanks.

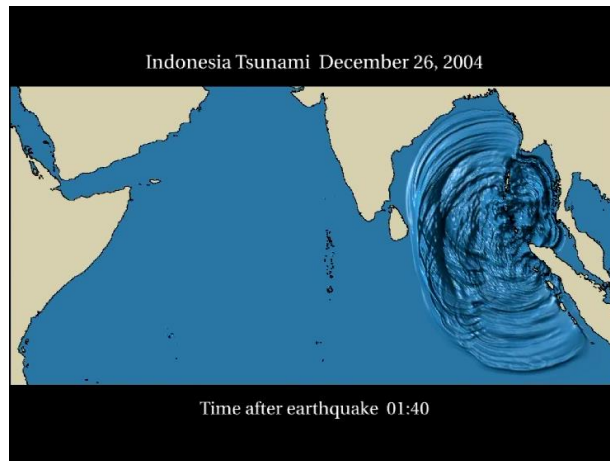


*Figure-movie 4.1 Indonesia tsunami Dec. 26. 2004 Indian Ocean Tsunami animation.*

[<CLICK HERE TO WATCH MOVIE \(top\\_2fps1.mp4\)>](#)

#### **GLOBAL INDIAN OCEAN TSUNAMI, 2004**

The movie below (Figure-movie 4.2), depicts the generation of the tsunami in the Indian Ocean in December 2004 and subsequent tsunami propagation in the entire World Oceans. The source function, i.e., the bottom uplift, has been described in Chapter 3, Sec.4. The movie is strictly related to Chapter 4, Secs. 5 and 6, where the physics of propagation is explained based on the calculated energy flux through cross-sections between Africa and Antarctica and Australia and Antarctica. The movie shows wave propagation in real-time. Initial bottom uplift generates a two-wave-systems, one is traveling to the East into Indonesian Islands, the second wave propagating to the west towards India, Maldives Islands, and the Atlantic Ocean, and the south towards Antarctica and the South Pacific Ocean. It is interesting to see that travel routes in the Global Ocean are not uniquely defined; therefore (important for the tsunami warning), travel time is also not uniquely defined. For example, the wave traveling to Alaska can arrive via Indonesian Islands in the shortest time; fortunately, with low energy. The second route leading via South Pacific (along ridges) will bring a tsunami a few hours later but with a much stronger signal. Observing the wave pattern between South America and Antarctica, one can see that the above wave is influenced by the signal coming from the South Atlantic (and vice versa, the

signal from the South Pacific influences the signal in the Atlantic). The movie also demonstrates how the distribution of continents influences the tsunami wave structure. We can observe that when the very chaotic signal from the Indian Ocean (due mainly to many reflections) arrives at the relatively narrow passage between Australia and Antarctica, it further propagates into the South Pacific as a well-structured wave. A similar change in tsunami signal is observed when a tsunami enters from Southern to Northern Atlantic. The movie was produced at the Arctic Research Supercomputer Center of University of Alaska, Fairbanks.

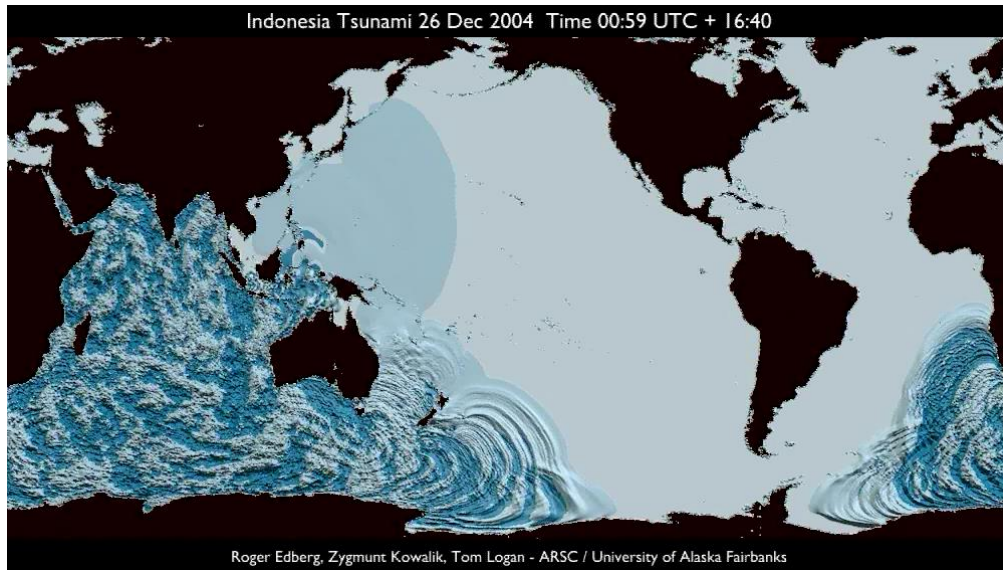


*Figure-movie 4.2 Global Ocean, Indonesia tsunami Dec. 26, 2004 animation.*

[<CLICK HERE TO WATCH MOVIE \(GLOBAL-FLAT-TITLED-RETIME02B\\_SMALL.MP4\)>](#)

### **KURIL PACIFIC TSUNAMI PROPAGATION, 2006**

The movie below (Figure-movie 4.3), depicts propagation of tsunami in the North Pacific in November 15, 2006. The source function, i.e., the bottom uplift/downdrop has been described in Fig. 4.22 of the text. The movie shows wave propagation for 14-hour time span. Initial bottom uplift generates two wave-systems, one traveling to the North-West into the Okhotsk Sea and the second wave propagates to the South-East towards Hawaii. The wave moving to the North Pacific is transformed by the large bathymetric features like Emperor Mountain Chain, Hess Rise, Koko Guyot, Hawaii Island and Mendocino Escarpment. The focusing by Mendocino Escarpment and Koko Guyot brings large waves to Crescent City, often a few hours after the first wave arrival. Time comparison between the measured sea level by two DART Buoys and computed by the model demonstrates that only the first few waves are well reproduced. Later arriving waves are badly reproduced due mainly to the coarse resolution bathymetry used in computations.

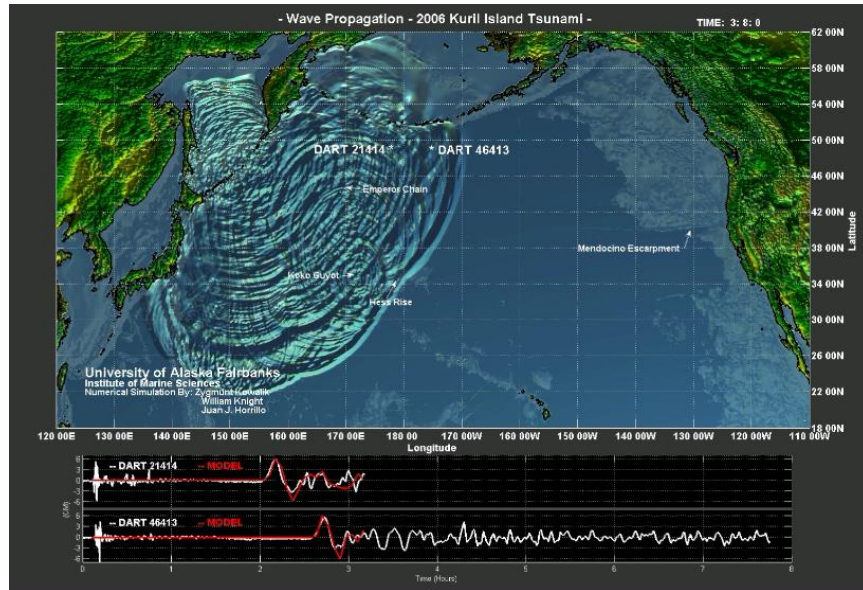


Figure-movie 4.3 Kurile tsunami Nov. 15, 2006 animation.

[<CLICK HERE TO WATCH MOVIE \(Northpac\\_kurile\\_small.mp4\)>](#)

### KURIL ENERGY FLUX

To further identify Koko Guyot as an important bathymetric feature, the non-linear shallow water wave equations were solved numerically on a 1 arc-minute grid and used to compute energy flux vectors in time. These are defined by Eqn. 1.52 in the text. A main energy lobe (first wave front) is observed once the tsunami wave arrives at Koko Guyot. A later circular expanding wave front, clearly centered on Koko Guyot, is seen to be scattered by the seamount. In this way, two closely spaced wave fronts are observed over the Northern Pacific. These are further enhanced by the Mendocino Escarpment. The two maxima can be easily tracked up to their arrival at Crescent City.

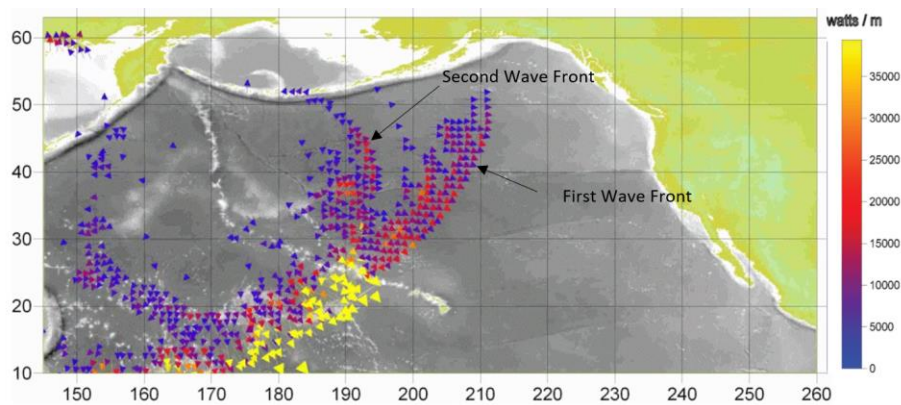


Figure-movie 4.4 Kurile tsunami energy flux animation.

[<CLICK HERE TO WATCH MOVIE \(kurile\\_energyflux.mp4\)>](#)

### GUYOT INSET:

Scattering dynamics are explored in more detail in a simplified 2D model geometry using Cartesian coordinates and the linearized shallow water wave equations. Coriolis terms were not included. The model domain is a 400 km X 400 km square at 1 km spatial resolution. The “ocean” bathymetry is flat at 5000 m depth. The guyot (a crude approximation of Koko Guyot) is a right cylindrical frustum with base radius equal to 60 km, located at the center of the model domain. The top, at 500 m depth, has a radius of 40 km. A 1m amplitude plane wave with 75 km wavelength and moving in the  $+x$  direction is incident on the guyot (Figure-movie 4.5)

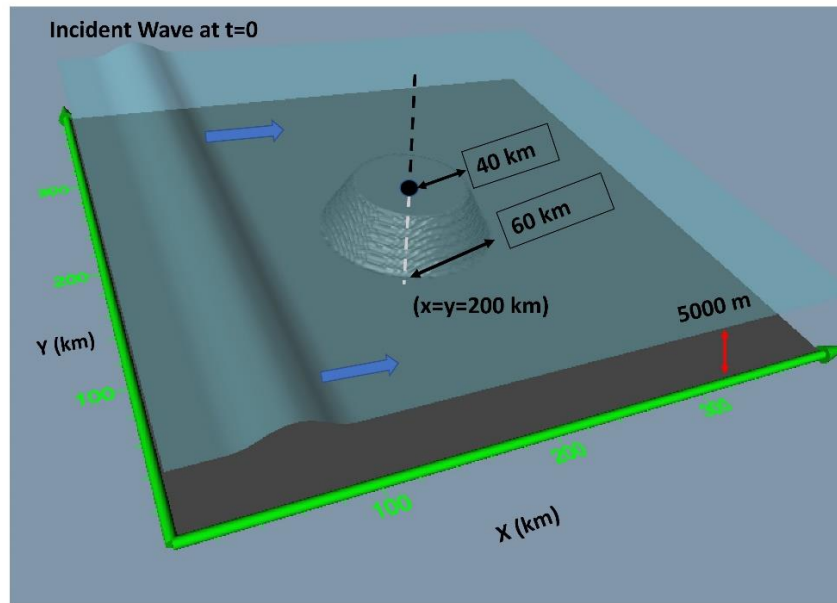


Figure-movie 4.5 – Guyot model geometry at  $t = 0$ .

[<CLICK HERE TO WATCH MOVIE \(Guyot\\_inset.MP4\)>](#)

Snapshots of the sea surface at defining moments are shown below in Figure-movie 4.6. The circular expanding wave front in Figure-movie 4.6, is identified as the scattered wave. The angular dependence of the energy flux (defined by Eqn. 4.10 and 4.11 in the text) is defined as the maximum energy flux passing through a circular mathematical surface of radius 250 km, centered on the point  $(x=340 \text{ km}, y = 300 \text{ km})$ . This point is located on the downwind edge of the guyot. The domain size was increased to 600 km X 600 km in order to better separate the incident and scattered wave fronts.

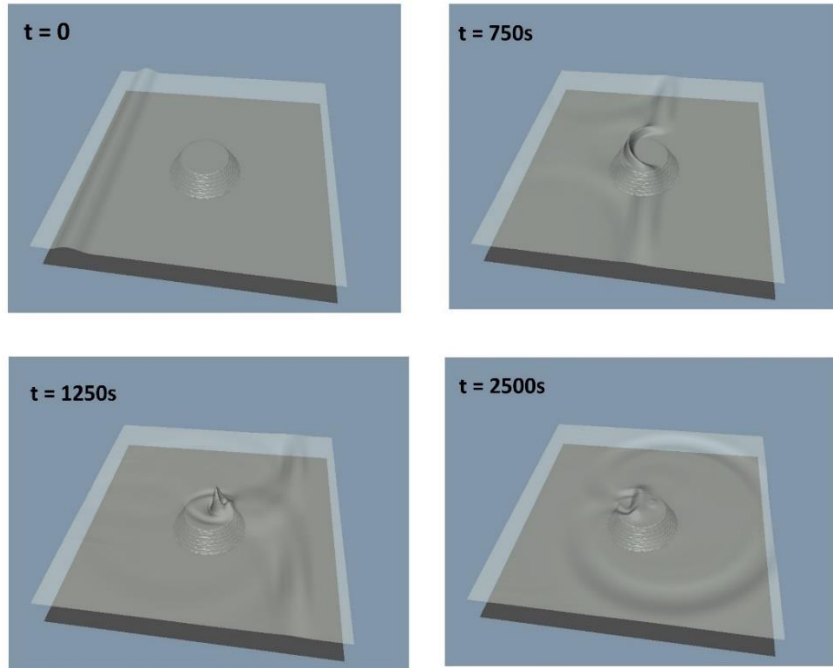


Figure-movie 4.6 – top\_left: prior to wave / guyot interaction, top\_right: refraction around top of guyot, bottom\_left: Max amplitude spike at downwind side of the seamount, bottom\_right: the slower wave atop the seamount, moving in the -x direction, wraps around the guyot, producing a nearly circular expanding wavefront.

The plot in Figure-movie 4.7 below shows the normalized scattering amplitude as a function of scattering angle. In this example the amplitude is the maximum energy flux passing through a circular mathematical surface of radius 250 km, centered on the point (x=340 km, y = 300 km). The scattered energy flux amplitudes are normalized to the incident wave value. Scattering towards Crescent City would be roughly at  $\theta = 100 - 110$  degrees

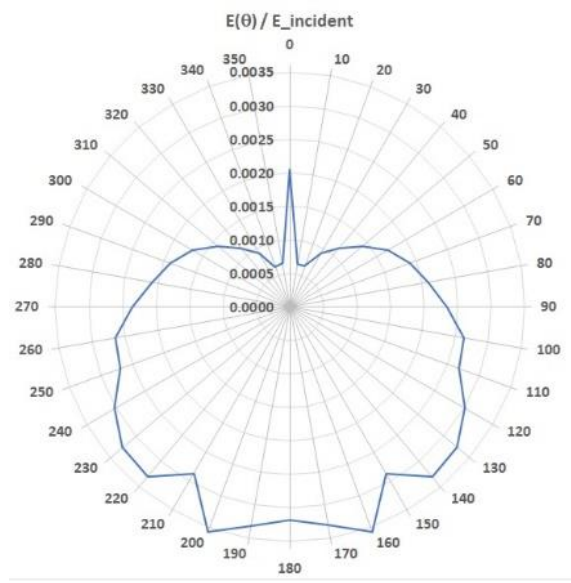


Figure-movie 4.7 – Maximum energy flux as a function of scattering angle. Theta = 0 corresponds to propagation in the -x direction. The flux is normalized to the incident wave energy flux

## CHAPTER V

### CHAPTER V – SECTION 5.2

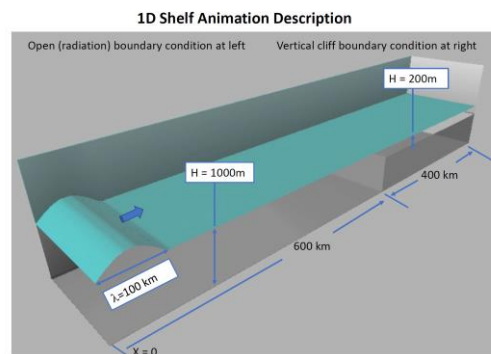
#### SHELF BREAK / TRAPPING

##### NARRATIVE - CONNECTION TO THE TEXT

Ch.V, Sec.2 considers two cases of tsunami running onto the shelf – the linear sloping bottom and a more realistic shelf profile from the Gulf of Alaska. These interactions resulted in reflected waves and trapped wave oscillations over the shelf. And as we see in Ch.IV descriptions of the Indian Ocean and the Kurile Islands tsunamis, the main reason for modifications of transoceanic wave propagation is the interaction of waves with bathymetric features such as shelves, oceanic ridges, and seamounts. This simple animation shows how the shelf break generates these behaviors.

##### MODEL DESCRIPTION

- The animation depicts the effect of a simple (sharp) shelf break on an incoming single wave, revealing trapping, reflection, and transmission of wave shape across a simple bathymetric discontinuity.
- This is a 1D, transient shallow water wave model  $u(x, t)$  and  $\zeta(x, t)$  – with no non-linear terms
- Spatial step size  $\Delta x$  is 1 km, time step is 1 s.
- Position along the  $x$  axis is denoted by  $x = \Delta x * i$  where  $i = 1, 2, 3, 4, \dots, 1000$
- The shelf break transition occurs within a single spatial step at  $i = 600$ . Note that the results are nearly identical if the transition occurs linearly over 5 steps ( $598 < i < 604$ ).
- 300 animation frames were generated at 100 s intervals - giving 8.3 hours of wave evolution
- The initial wave form is the positive half of a sinusoid with  $\lambda = 200$  km and  $\zeta(x, 0) = \text{SIN}(2\pi x / \lambda)$  for  $0 < x < 100$  km, and  $\zeta(x, 0) = 0$  elsewhere



[<CLICK HERE TO WATCH MOVIE \(ShelfBreak.mp4\)>](#)

Figure-movie 5.2.1 – Wave trapping and reflection by a continental steep shelf break.

## MODEL SUMMARY

Sea level time series for two “numerical gages” (blue is taken at  $i = 400$  in deep water and red at  $i = 650$  in shallow shelf water). Note that the transmitted and reflected wave amplitudes track well with predictions in Chapter 2, sec 1 **Fig 2.2 and eqn 2.7**

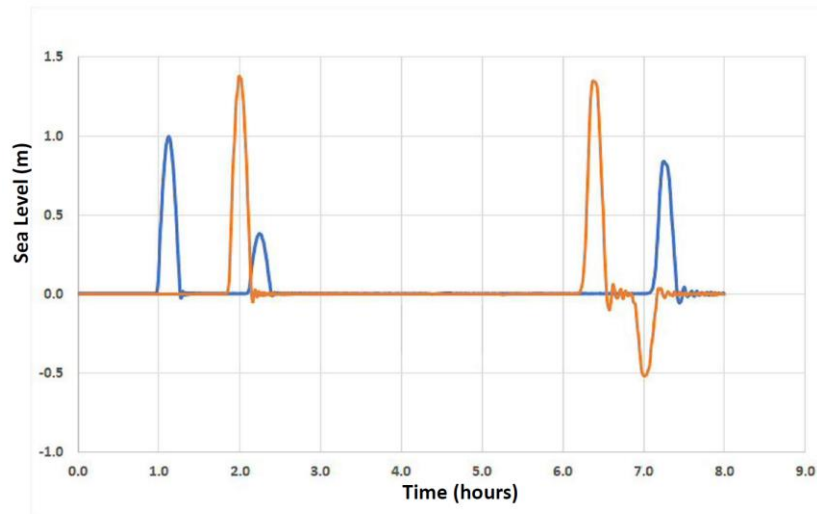


Figure-movie 5.2.2 –Transmitted and reflected wave comparison. Deep water (red) and shallow water (blue).

## CHAPTER V - SECTION 5.2

### IMPLICATIONS OF RUNUP

#### NARRATIVE - CONNECTION TO THE TEXT

The tsunami traveling towards the shoreline interacts with the bathymetry. The shallow water slows the tsunami signal down, magnifying its amplitude and velocity. We consider the linear profile given in Figure 5.1 of the textbook (Figure-movie 5.2.3).

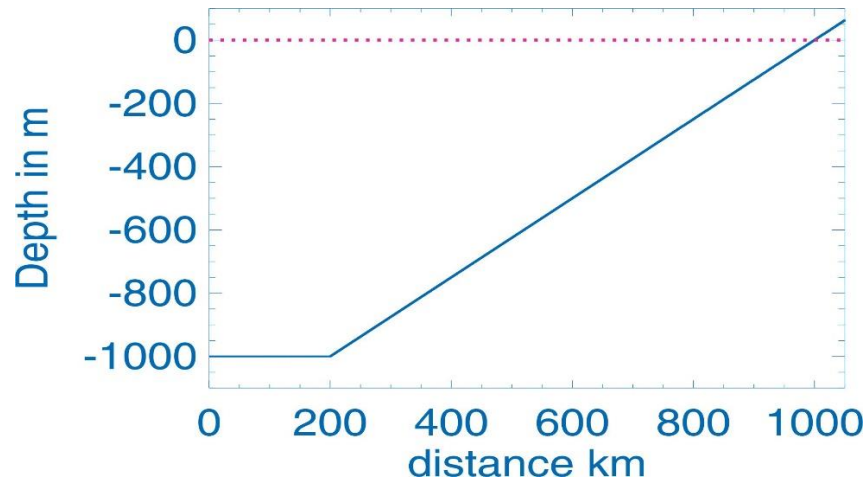


Figure-movie 5.2.3. Linear bottom profile.

The tsunami is generated by the uplift of a 100 km long segment of ocean bottom between 50 and 150 km from the open boundary at a depth of 1000 m. The initial wave height is 200 cm, and as the wave propagates to the open boundary and to the sloping bottom, it splits into two waves of 100 cm. The initial boxcar signal profile traveling up slope undergoes two changes; its wavelength steadily shortens, and its amplitude grows. Arriving at the shoreline, it generates a runup. The reflected wave from the shoreline lost its boxcar profile and resembled an oscillatory wave, see Figure-movie 5.2.4.

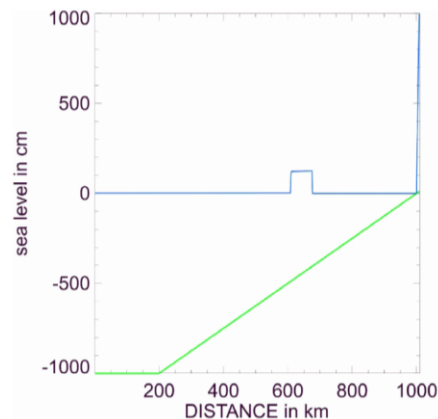


Figure-movie 5.2.4. Transformation of a square tsunami wave on an upslope channel

[<CLICK HERE TO WATCH MOVIE \(TSUNAMI.MP4\)>](#)

The wave traveling towards the open boundary undergoes similar transformations as the boxcar signal. However, in reverse order, i.e., the large amplitude diminishes, and the wavelength continuously increases while the wave propagates toward the left open boundary. This experiment shows the importance of bathymetry in generating reflected (secondary) tsunami signals. The periods of the secondary waves are defined by reflection and by the generation of new modes of oscillations through an interaction of the tsunami waves with the shelf/shelf break geometry. The previous movie (Figure-movie 5.2.4) shows the tsunami traveling 800 km upslope and downslope in the channel. The next movie (Figure-movie 5.2.5) describes domain located between 980 km and 1010 km, where channels changes from water to 50 m on land (dry domain).

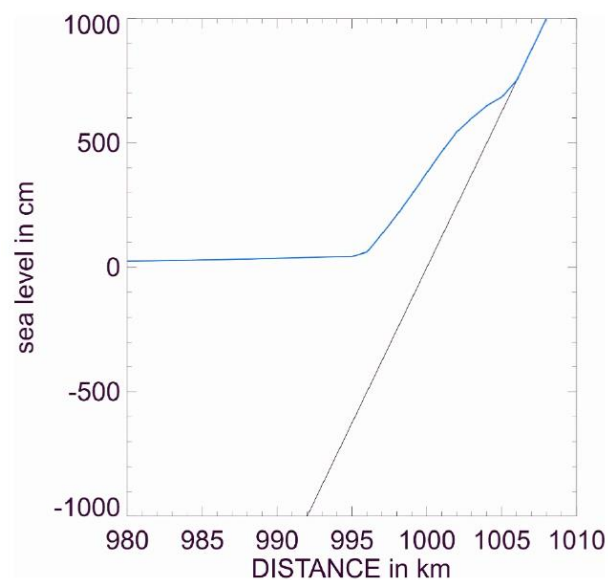


Figure-movie 5.2.5. Transformation of a square tsunami wave on an upslope channel

[<CLICK HERE TO WATCH MOVIE \(TSUNAMI RUNUP AND RUNDOWN.MP4\)>](#)

The detailed process of wave amplification when it travels up and down the beach can be observed. The domain and the runup of 8.5 m amplitude and rundown of -5 m are shown in Figure-movie 5.2.6

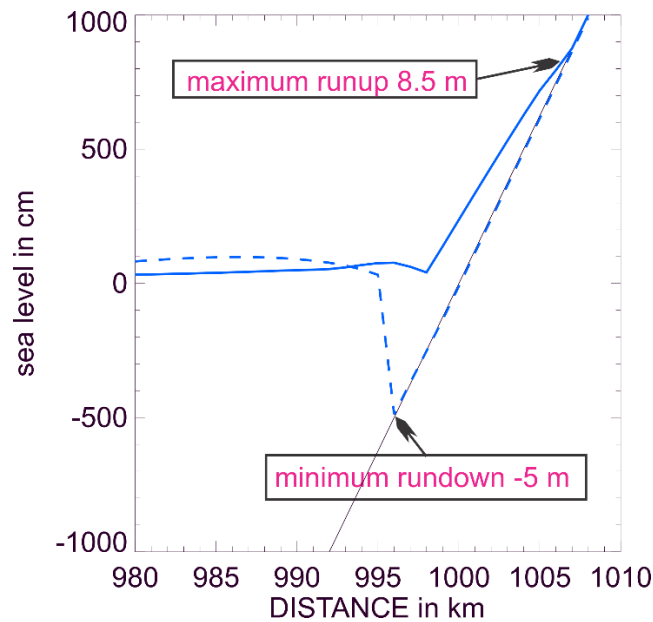


Figure-movie 5.2.6 Tsunami traveling up the beach (8.5 m) and down the beach (-5 m). This is the upper part of the channel depicted in Figure-movie 5.2.3

## MODEL DESCRIPTION

The one-dimensional models from Chapter 1 serve as a base for the present experiments on tsunami propagation and runup. The equation of motion includes all terms, and only Coriolis force is neglected. The Fortran program developed for the runup study titled: `runup_beach.f90` (see the textbook, page 93) has been modified to include tsunami generation. In the original program, the wave enters the channel through the left open boundary. In the modified program, the radiation condition governs this boundary. When the bottom uplift generates a tsunami, the wave moving to the left is radiated outside by this condition. The spatial grid of 10 m resolves the wave in the channel of 1000 km (100000 grid points). The boxcar tsunami signal of 100 km long is well resolved, but the boxcar is not a sinusoidal signal. It is important to resolve the steep front and back of such a signal. Practically, one can always expect some dispersive waves at both ends. This process is stronger in shallow water. Figure-movie 5.2.7 describes the enhancement and the changes at both ends of the boxcar signal in the channel. The wave arriving at the beach reveals even stronger deformation (Figure-movie 5.2.8). The question is why the front of the wave is much less distorted than the back. In shallow water, along with the dispersion, the total depth (which includes both depth and sea level) changes the wave speed at the bottom and the top of the signal, thus resulting in additional deformation.

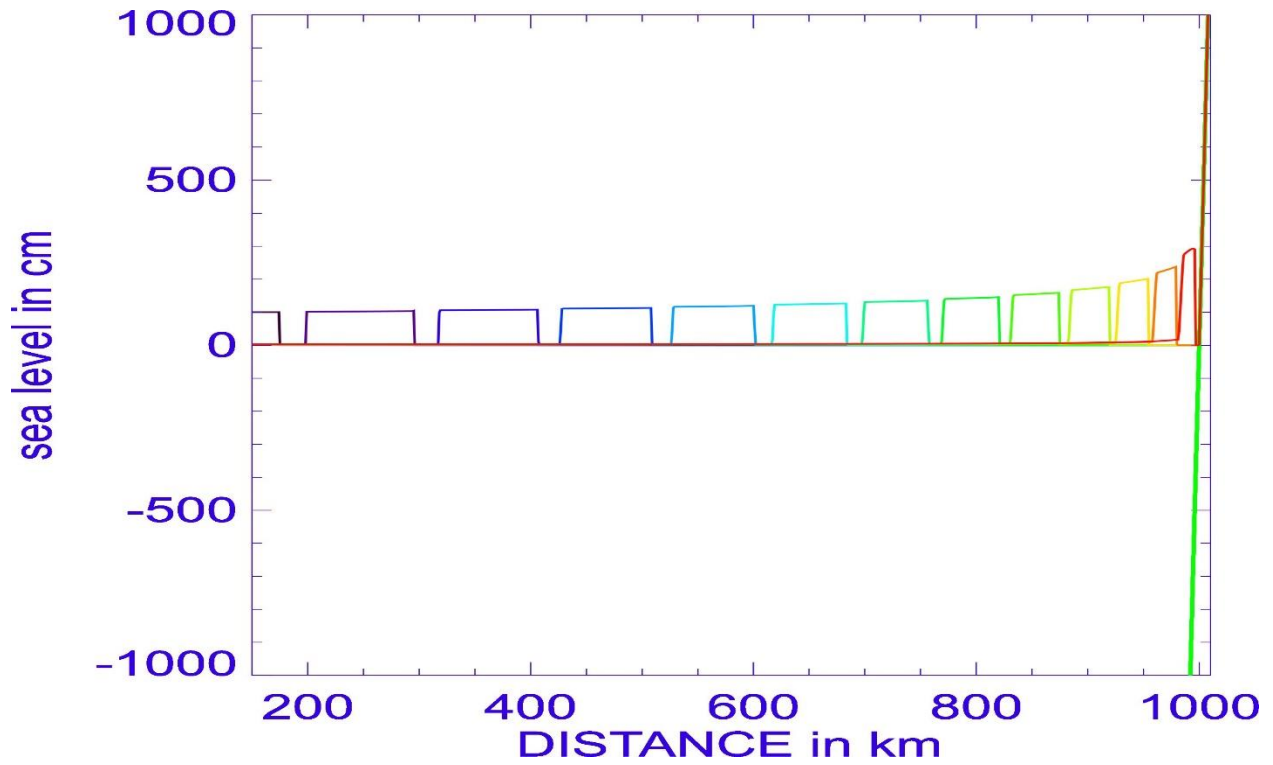


Figure-movie 5.2.7 The amplification and distortion of the boxcar signal. Different colors show the movement of the signal toward the shore.

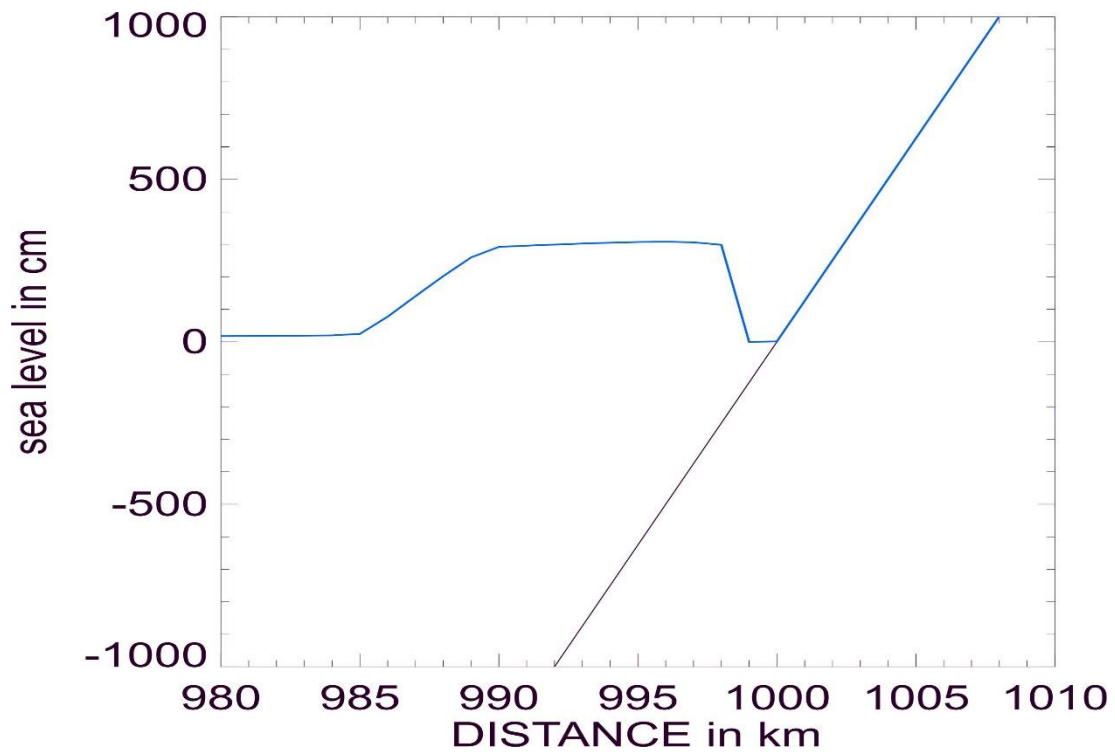


Figure-movie 5.2.8 Tsunami in close proximity to the beach. The front and the back of the boxcar signal show different distortion.

## **MODEL SUMMARY**

This experiment shows the importance of bathymetry in generating reflected (secondary) tsunami signals. The periods of the secondary waves are defined by reflection and by the generation of new modes of oscillations through an interaction of the tsunami waves with the shelf/shelf break geometry. The boxcar tsunami signal interacting with the sloping bottom generates oscillatory signals of different shape from the initial boxcar. The distortion at the front/back of the wave could be attributed to a combination of shoaling (at the front of wave), reflection and dispersion (at the tail of the wave).

## CHAPTER V - SECTION 5.7

### IMPLICATIONS OF SHELF BREAK MORPHOLOGY

#### NARRATIVE - CONNECTION TO THE TEXT

Chapter 5, Sec.5.7 considers the effect of both shelf and coastal configuration centered on Crescent City, CA. Due to their curvatures, wave trapping, focusing and its resulting amplification are possible. This animation shows how a simple curved shelf break can produce both amplification and modulation of maximum wave amplitudes along a simple straight coast.

#### MODEL DESCRIPTION

- This is a 2D, transient shallow water wave model  $u(x, y, t)$ ,  $v(x, y, t)$ , and  $\zeta(x, y, t)$  – with no non-linear terms
- The spatial step sizes  $\Delta x$  and  $\Delta y$  are 1 km. The time step is 1 s.
- Position along the  $x$  and  $y$  axes is denoted by  $x_i = \Delta x * i$  where  $i = 1, 2, 3, 4, \dots, 500$  and  $y_j = \Delta y * j$  where  $j = 1, 2, 3, 4, \dots, 500$
- 150 animation frames were generated at 200 s intervals - giving 8.3 hours of wave evolution.
- The initial right moving wave is the positive half of a sinusoid, where  $\zeta(x, 0) = a * \text{SIN}(2\pi x / \lambda)$  for  $0 < x < 160$  km, and  $\zeta(x, 0) = 0$  elsewhere. The amplitude  $a$  is 0.25m, and  $\lambda = 320$  km
- The shelf break (see figure-movie 5.7.1) is parabolic in shape according to  $x = 4h \frac{(y - \frac{Ly}{2})^2}{Ly^2}$  with a central “bulge”  $h$  of 150 km.  $Ly$  is the domain width (500 km). The abrupt transition from 1000m to 62m depth is smoothed over  $2\Delta x$ . Considered as a *lens*, the apparent focal length (FL) is seen in the model results to be  $\sim 310$  km. This analogy can only be approximate because a true focus would produce an extremely tall and steep mound of water- which would expand radially prior to reaching that point.
- An interesting aside is that treating the shelf break as a lens and using Snell’s Law with  $\sqrt{\frac{a_1}{a_2}}$  playing the role of index of refraction gives results similar to the model. FL in this case varies somewhat along the length of the shelf break, but within 125 km of the domain centerline, the FLs are between 280 and 330 km, bracketing nicely the model results.

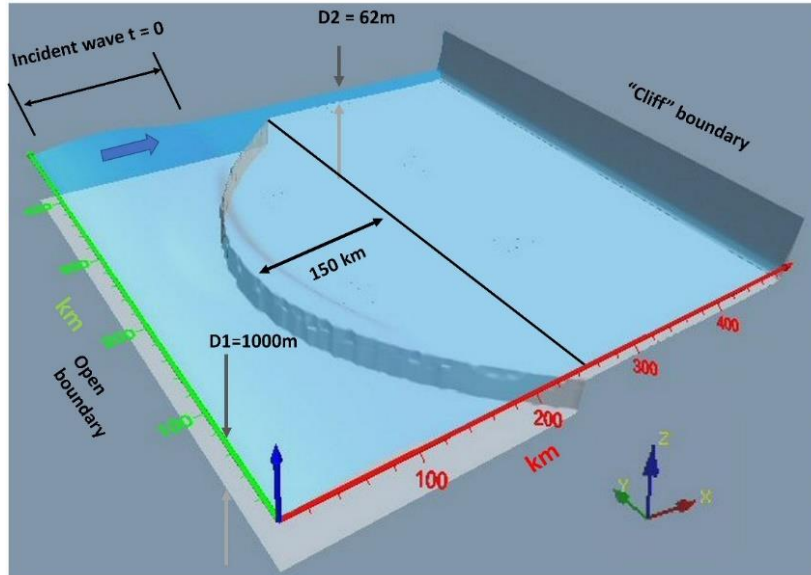


Figure-movie 5.7.1 Convex shelf break and straight cliff boundary

[<CLICK HERE TO WATCH MOVIE \(SHELFBREAKMORPH.MP4\)>](#)

#### MODEL SUMMARY

In this animation (Figure-Movie 5.7.1), the shelf break has curvature while the coast is straight ( $x = \text{constant} = 500 \text{ km}$ ). During the time leading up to coastal impact and 1 hour following reflection back towards the shelf break, the maximum wave amplitude occurs along the domain centerline at  $y = 250 \text{ km}$ . The tan-colored mathematical cut-plane ( $x$ - $z$  plane) seen in the animation is placed at the model centerline to display the wave profile more clearly. Model results are also depicted in Figure-movie 5.7.2, showing the effect of wave focusing on amplitude and resulting impact at the coast.

In the absence of shelf curvature, the modeled coastal impact would be uniform across the length of the coast. Prior to arrival however, the wave front is curved such that the first impacts occur close to both coastal edges which then move towards the center of the coast over a period of 41 minutes. This can be seen in the animation as what appears to be a pair of diaphanous waves moving along the coast and converging at the center. Figure-movie 5.7.3 shows this wave arrival dependence on time and location. Note the gray curve corresponds to the moment of maximum coastal amplitude.

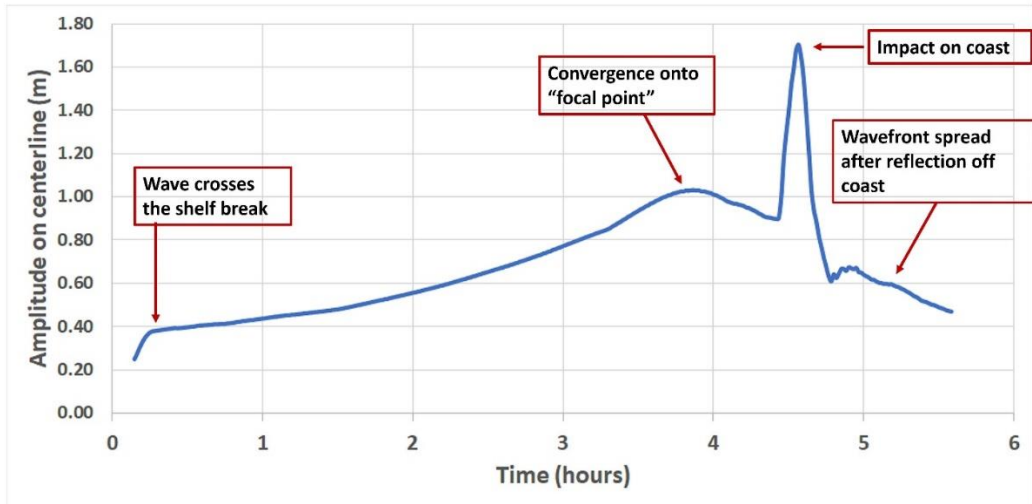


Figure-movie 5.7.2 Maximum wave amplitude at  $y=250$  km

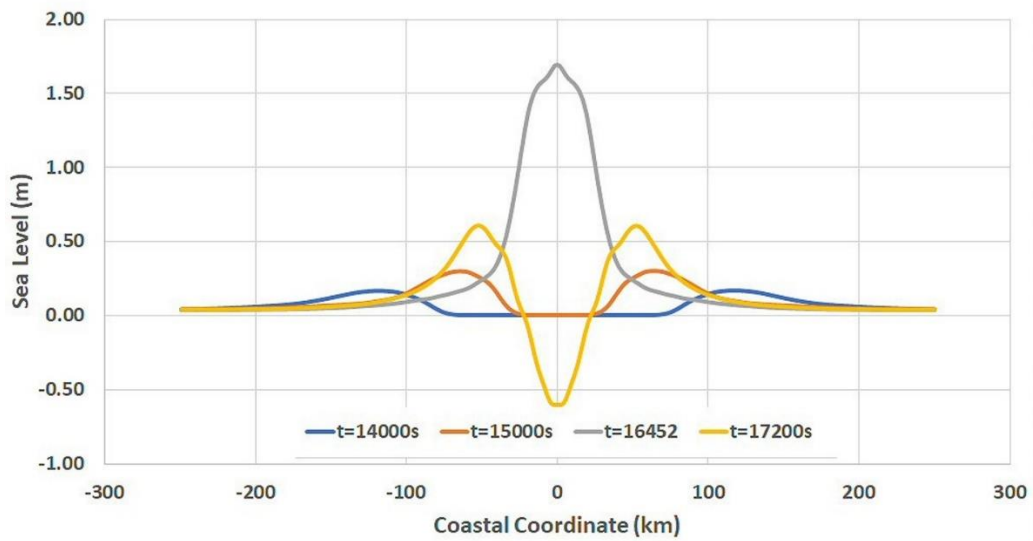


Figure-movie 5.7.3 Coastal impact (coastal coordinate as measured from centerline)

Reflector: This is the parabolic coastline reflection.

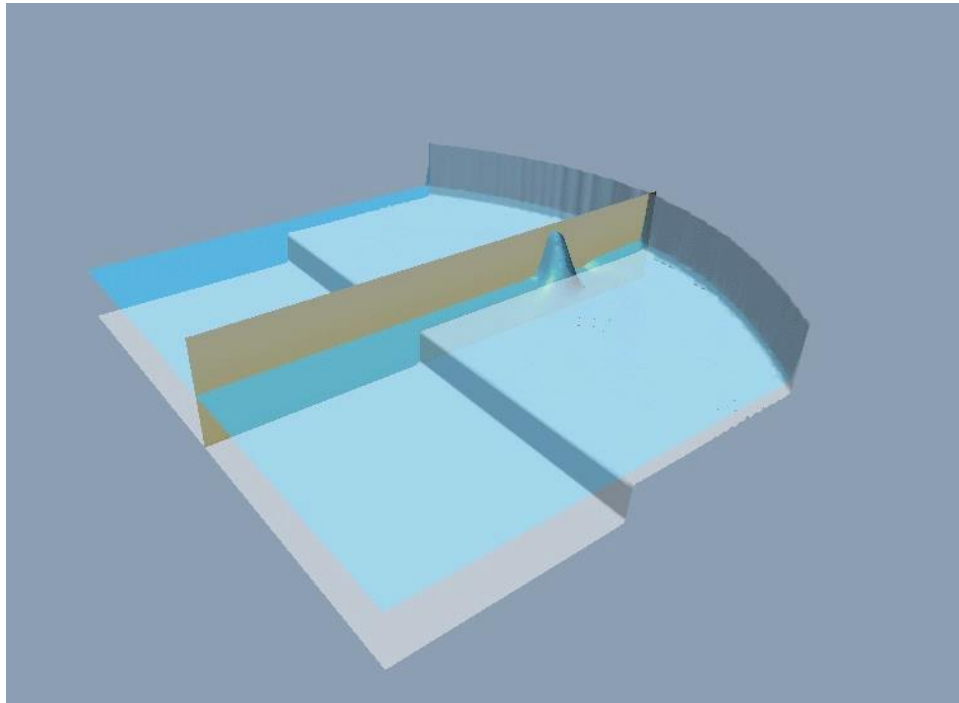


Figure-movie 5.7.4 Straight shelf break and concave cliff boundary.

[<CLICK HERE TO WATCH MOVIE \(Reflector.mp4\)>](#)

The animation (Figure-Movie 5.7.4) shows an interesting reversal of the original model geometry where shelf break and coastal details have been interchanged. The coast now has curvature while the shelf break is straight and oriented perpendicular to the incident wave. The remaining parameters are unchanged. Note that there is a similar focusing behavior due not to refraction in this example, but to coastal reflection. Figure 5.14 of the text displays bathymetry near Crescent City, California that contains elements of both animations – curvature of both coastline and shelf break.

## TSUNAMIS AND GEOMETRIC OPTICS

### NARRATIVE - CONNECTION TO THE TEXT

Section 5.7 also introduces *rays* into the explanation of wave periods observed at Crescent City, California. In this context, each length element of a wave front is considered to have a ray associated with it - a 2D vector perpendicular to the local wavefront and parallel to the direction of propagation. Its magnitude can be thought of as the local phase velocity. Rays, a concept found in geometric optics, have remarkable predictive utility in understanding shallow water wave propagation. They are also useful in many qualitative predictions of tsunami wave behavior. Their close connection to tsunamis is demonstrated in this animation of wave propagation in an “ocean” of *uniform depth*. The coastline, shown in figure-movie 5.7.5, is elliptical with semi-major axis of 480 km ( $X_m$ ) and semi-minor axis of

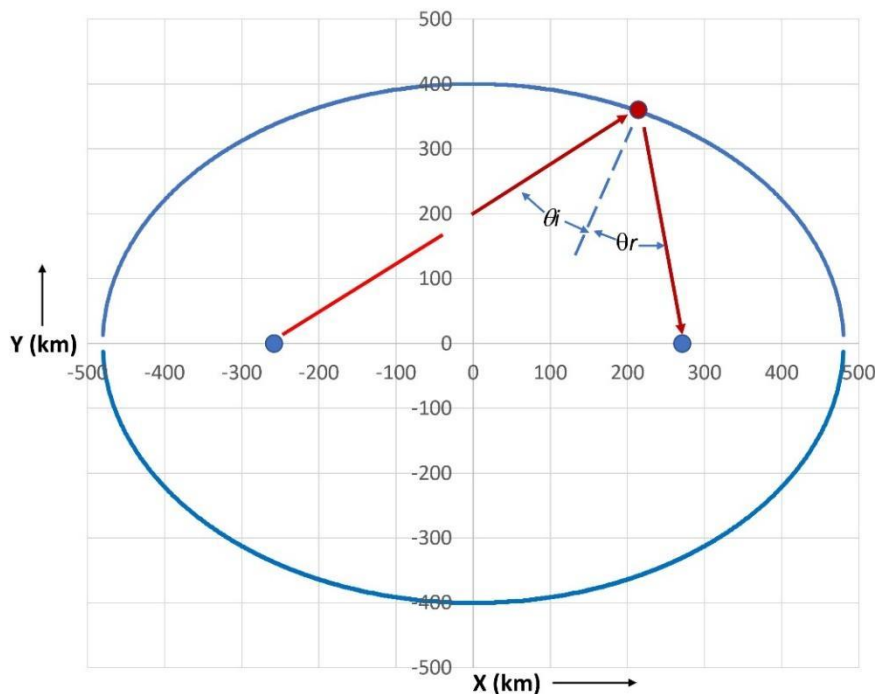


Figure-movie 5.7.5- model geometry and representative ray path

400 km ( $Y_m$ ). The two ellipse foci are located at  $y=0$ ,  $x=\pm 265$  km. A ray, drawn in red, leaving the left focus, is reflected to the right focus (anticipating  $\theta_i = \theta_r$ ). The sum of the two path lengths is a constant for any coastal point. This results in all rays departing the left focus at  $t=0$  converge simultaneously on the right focus, leading to wave reinforcement.

These analytical results provide a useful model test.

### ELLIPTICAL OCEAN MODEL DESCRIPTION

- This is a 2D, transient, shallow water wave model, with variables  $u(x, y, t)$ ,  $v(x, y, t)$ , and  $\zeta(x, y, t)$ . Non-linear terms, friction, and Coriolis forces have not been included. The model is developed in the Cartesian system of coordinates.
- Spatial step sizes  $\Delta x$  and  $\Delta y$  are set to 1000 m, and the time step is 1/2 s.
- “Ocean” depth is uniform at 5000m, giving a wave phase speed ( $c = \sqrt{gH}$ ) of 221 m/s
- Position along the  $x$  and  $y$  axes is denoted by  $x = \Delta x * i$  where  $i = 1, 2, 3, 4, \dots, 1000$  and  $y = \Delta y * j$  where  $j = 1, 2, 3, 4, \dots, 1000$
- Initial conditions are:  $u = v = 0$ . Setting  $r^2 = x^2 + y^2$ ,

$$\zeta(x, y) = A_o \cos^2 \left( \frac{\pi r}{2 r_o} \right), \text{ for } 0 < r < r_o$$

$$= 0, r > r_o$$

where  $A_o = 40$  m and  $r_o = 40$  km

The coastal equation for the model ellipse is

$$\left( \frac{x}{X_m} \right)^2 + \left( \frac{y}{Y_m} \right)^2 = 1$$

- 85 animation frames were generated at 100 s intervals - giving 2.4 hours of wave evolution. This allows the initial sea level disturbance to transit from left to right focus and back again to the left focus starting point.

#### MODEL SUMMARY

Snapshots of the wave propagation from the source at the left focus to first arrival at the right focus in shown below in Figure-movie 5.7.6

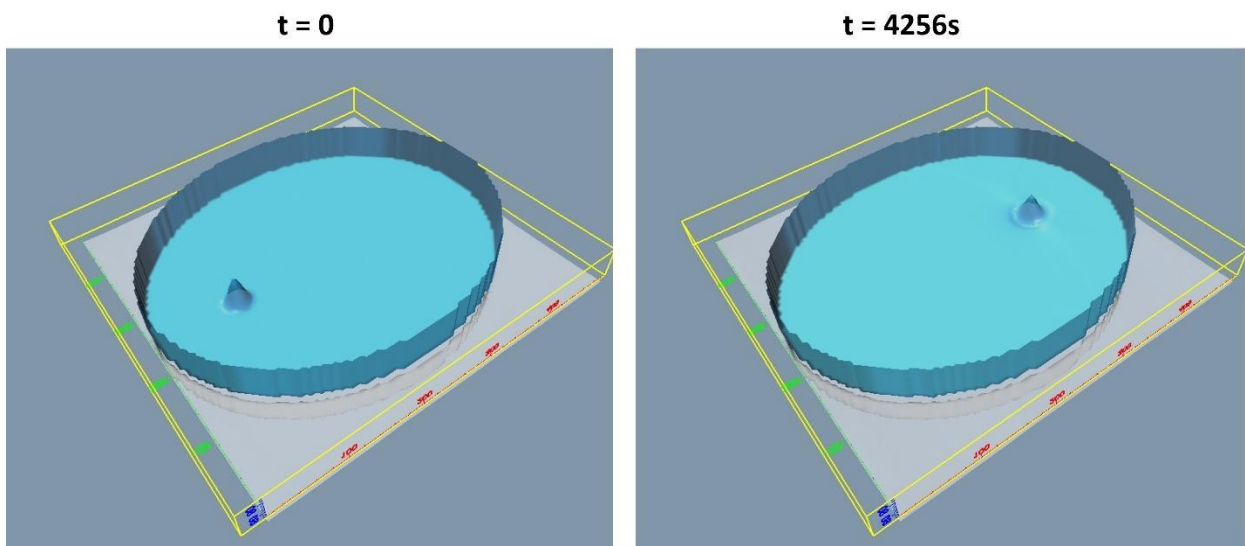


Figure-movie 5.7.6: Maximum Amplitudes at two foci – source located at left focus

[<CLICK HERE TO WATCH MOVIE \(Ellipse.mp4\)>](#)

The analytically derived prediction has the initial source disturbance converging onto the right focus, located at  $y = 0, x = 265$  km. The model result is identical to within the 1 km grid resolution. The expected wave travel time between foci is  $\tau = \frac{2X_m}{c} = 4335$ s. The model result for travel time to maximum amplitude at the right focus is 4256s – an under-prediction of 1.8%. Model plots of sea level taken along the x-axis,  $\zeta(x, y = 0, t = 4256s)$ , in Figure-movie 5.7.7 clearly show the presence of dispersion. A more pronounced dispersive tail develops during the second transit from right focus back to the left focus.

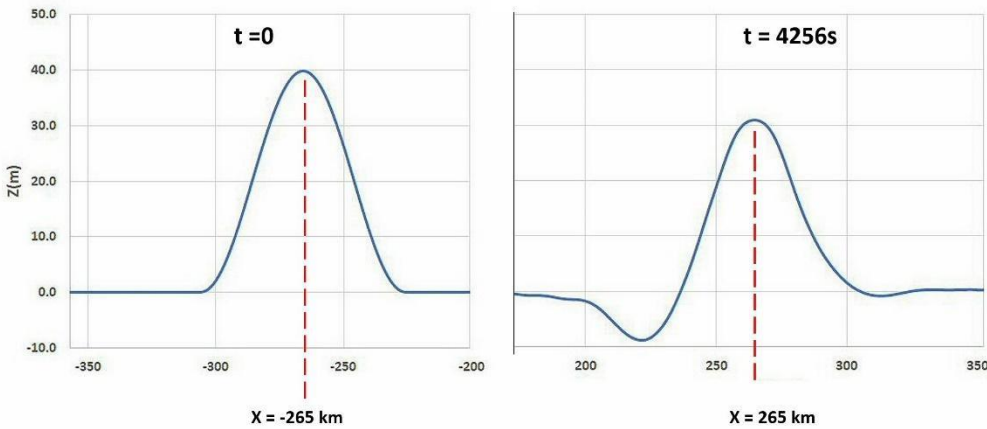
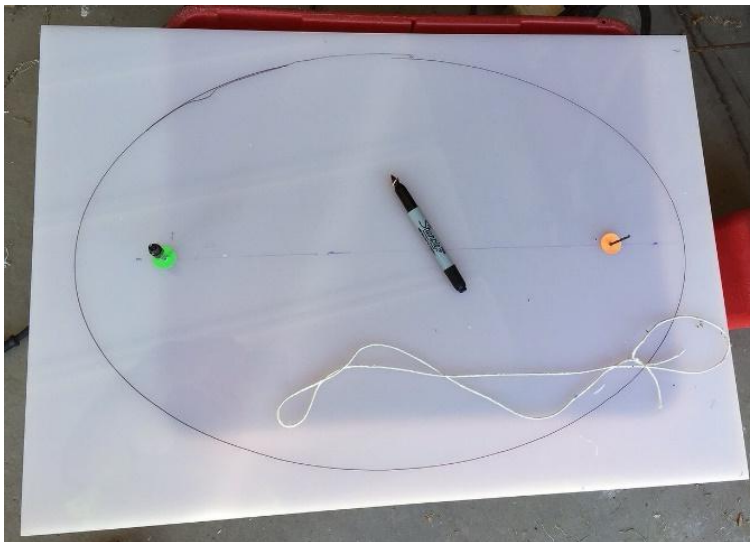


Figure-movie 5.7.7 Maximum Amplitudes at two foci

### AN EXPERIMENTAL RESULT



A simple physical model with elliptical geometry was constructed from plastic parts in a garage (figure 5). The semi-major axis is 28 cm and semi-minor axis is 19cm. The tank was flooded to 3 cm depth with tap water. Colored sticky dots locate the two foci. A movie of wave motion from left focus to right can be seen by clicking on the link below. Motion can be seen continuing through several cycles

Figure movie 5.7.8 – experimental elliptical tank

[CLICK HERE TO WATCH MOVIE \(EllipseMovie\\_2.mp4\)>](#)

## CHAPTER VI

---

### NARRATIVE - CONNECTION TO THE TEXT

Analysis of the data recorded during the Indian Ocean Tsunami of December 2004, and Japan Tsunami, 2011 demonstrated that the tsunami waves were noticeably dispersive. As the initial wave propagates, separation of the wave into spectral components with different frequencies and amplitudes occurs. Thus, the leading wave is followed by a train of waves formed in its wake. This train of waves interacts in coastal regions with the leading wave runup, drawdown, and reflection from shelf or from land, introducing strong modification to leading wave effects.

### MODEL DESCRIPTIONS

To show the dispersive properties of tsunami and the limitations of the nonlinear shallow water (NLSW) approach, three different models are compared: NLSW, nonlinear Boussinesq (NLB) and full Navier-Stokes equation aided by the volume of fluid method (FNS-VOF). Small domain encompassing the south part of the Bay of Bengal is used for the numerical simulations. Comparisons are made between NLB and NLSW models to uncover dispersive effects.

Figure-movie 6.1 shows the wave pattern at time 1 h 40 min using nonlinear shallow water (NLSW) and nonlinear Boussinesq (NLB) approaches. Due to dispersion effects, the NLB model features a pronounced series of waves trailing behind the leading wave. The wave pattern is significantly different from that of the NLSW model. From the NLB model results, it is seen that the length of the wave train is longer in the western region than in the eastern region (close to Thailand and Indonesia).

As Eqs. (6.1), (6.2) and (6.3) suggest (Chapter 6, Sec. 6.2.2), the magnitude of the dispersive term is proportional to the square of the water depth, and therefore the dispersion effect in the western region ( $H = 4$  to  $5$  km) is much stronger than in the eastern region (which is only of several hundred meters deep). Dispersive effects are also enhanced in the western region by the greater distance of propagation. Table below (textbook 6.2) gives model setup information and computer performance on a PC desktop single CPU computer (2006).

Table 6.2 Parameters for the numerical computation for the two-dimensional case (Bengal basin case).

Model	$\delta x$	$\delta y$	$\delta t$	Num. of cells	CPU time
NLSW	1 min	1 min	3 s	1249600	16.0 min
NLB	1 min	1 min	3 s	1249600	1.5 h

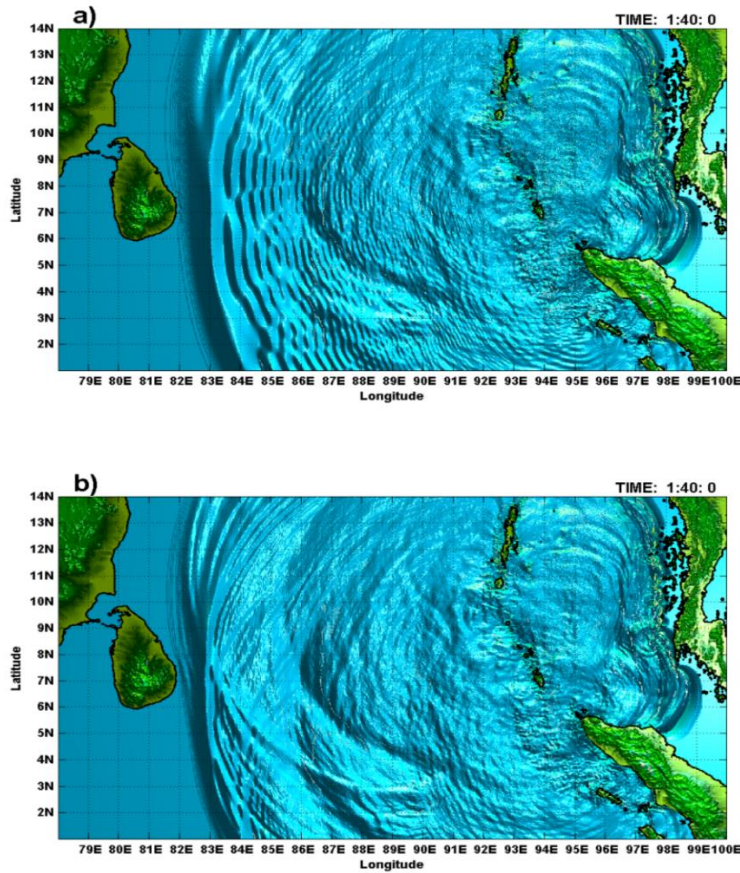


Figure-movie 6.1 Comparison of water surface computed at 1 h 40 min from the onset of the earthquake: a) 2D NLB model results, and b) 2D NLSW model results

[<CLICK HERE TO WATCH MOVIE \(NLSW\\_NLB\\_small\\_new.mp4\)>](#)

A simplified additional study is incorporated in which one-dimensional channels are used again to reveal the dynamics of dispersive wave runup. Model setup for this study is given in the following table

Table 6.1 Parameters for the numerical computation along transect A-A (channel case).

Model	$\delta x$	$\delta z$	$\delta t$	Num of cells	CPU time
NLSW	100 m	—	0.2 s	157059	30 m
NLB	100 m	—	0.2 s	157059	5 h
FNS-VOF	5 – 875 m	.2 – 40 m	(.08 – .8) s	800000	72 h

Figure-movie 6.2 shows the free surface snapshot at time 1 hour 20 min (4800 sec) from the onset of the earthquake of the Indian Ocean Tsunami (IOT) by three numerical models, 2D

Full Navier-Stokes (FNS), 1D NLB and 1D NLSW. The IOT propagation is based on the initial free surface deformation given by Fig. 3.9 of the textbook. General features of the wave evolution agreed very well in all approaches. However, some differences in reproducing the dispersion phenomena become noticeable as time advances (see movie). For instance, at time 40 min (2400 sec), wave dispersion is evident in the NLB and FNS-VOF results. A train of waves, imparted by the multiple frequency components of the leading wave, is formed just behind the leading wave. However, major wave features are well reproduced by the NLSW with the exception of the trailing wave train. The leading wave is taller and shifted forward in space relative to the dispersive approaches. The nondispersive NLSW approach overpredicts wave height. A slight advance in time of the NLSW leading wave crest is observed as well. However, the tip of the wave front of the NLSW leading wave matches very well with its dispersive counterparts. This reaffirms the use of NLSW as an accurate candidate for determining the tsunami arrival time.

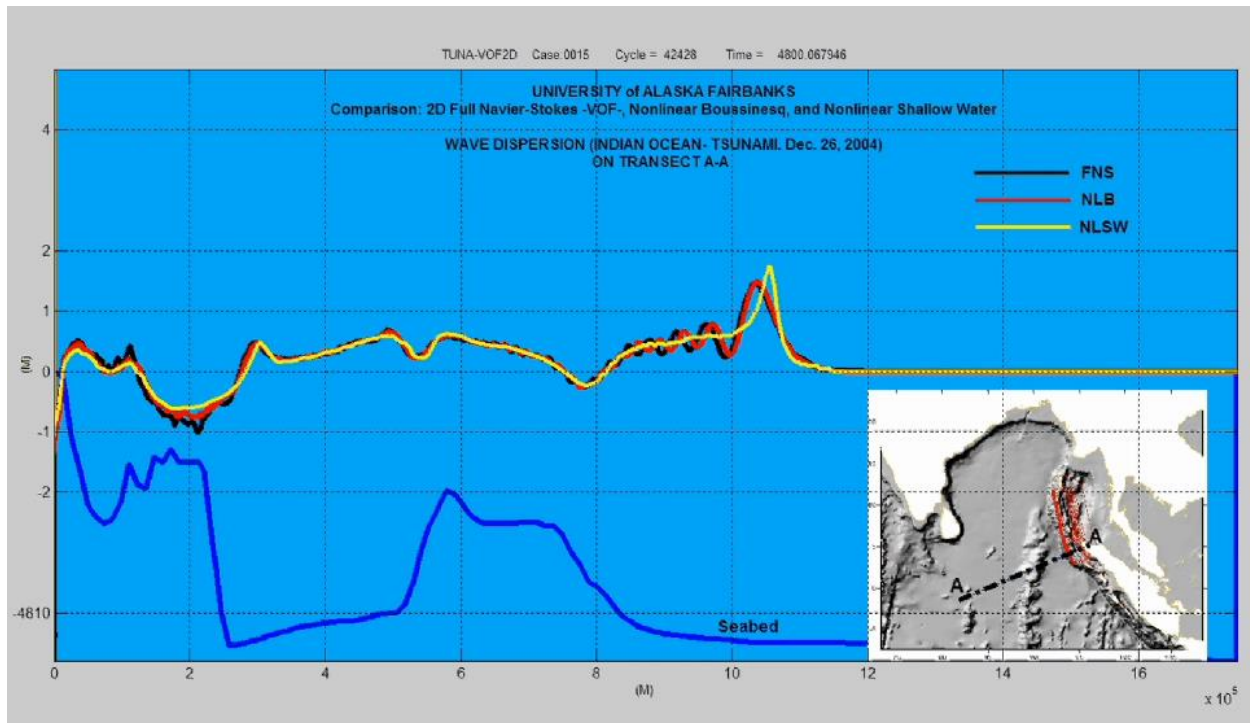


Figure-movie 6.2 Comparison of water surface computed by three models (2D Full Navier-Stokes (FNS), 1D NLB and 1D NLSW) at 1 hour 20 min (4800 sec) from the onset of the earthquake. Notice that the time plot is running in the opposite direction.

[<CLICK HERE TO WATCH MOVIE \(CASE\\_0015NEW1.MP4\)>](#)

## MODEL SUMMARY

Comparison of the three different methods shows that for practical purpose the NLSW model results are quite reliable since this model gives consistent results with its counterparts. The NLSW approach is very attractive nowadays for tsunami calculation because this method has very low computational cost. In addition, maximum wave height and runup are often overpredicted, increasing the safety factor. The NLSW results are useful for preliminary hazard assessment, where a simple and quick estimation of maximum wave

height, maximum run-up, and locations of maxima are required. Accuracy of location of the wave front tip for the IOT is excellent, reaffirms its use as a method for determining the tsunami arrival time. Qualitatively and quantitatively, the wave fronts reproduced by the NLB and FNS-VOF solutions share many common features. For longer integration times, the similarity holds only for the main maximum, because the phase difference between secondary maxima increases with travel time.

## CHAPTER VII

### SIMPLIFIED VOF (Volume of Fluid) FREE SURFACE RECONSTRUCTION FOR THE DAM-BREAK PROBLEM

#### NARRATIVE - CONNECTION TO THE TEXT

Modeling complex surface or interface evolution requires techniques that deal with multiple phases or separation of fluid. Examples which facilitate the understanding of these techniques include simulation of breaking waves or dam breaking. For these simulations the full Navier-Stokes and continuity equations are to be solved which also include the pressure field variable, in addition to the velocity field. The free surface or interface tracking is described by the discrete VOF function, and the fluid is advected as a Lagrangian invariant. In our notation this is the function  $F$ , see Chapter VI p. 268 and Chapter VII p. 322

#### MODEL DESCRIPTION

- This is a 2D time dependent Navier-Stokes model  $u(x,z,t)$ ,  $w(x,z,t)$  and  $F(x,z,t)$ . Spatial step size  $\Delta x$  is 1 cm,  $\Delta z$  is 0.5 cm and time step is 0.01 s.
- The inclusion of the vertical direction in the physics is an improvement for the solution of the dambreak problem as is the inclusion of the pressure
- Domain size is 40 cm by 20 cm
- The initial dambreak free surface is defined as step function at  $t=0$
- The animation depicts the determination of the  $F$  function in time

#### MODEL SUMMARY

In this particular 2D dambreak case, the standard VOF method of Hirt and Nichols [1981] for tracking the evolution of fluid interface has been simplified to clarify its concept. Here, only the concentration of the fluid ( $F$ ) is determined by using the transport or concentration equation at each of the computational grid or cell. A value of  $F=1.0$  (dark blue) indicates a full filled cell and value of  $F=0$  (white) indicates an empty cell and a value  $0 < F < 1$  indicates a surface cell (blue saturation). The surface interface (black line) is calculated by merely using a contour line at the value of 0.5. This is the simplest approach for surface reconstruction using the VOF method.

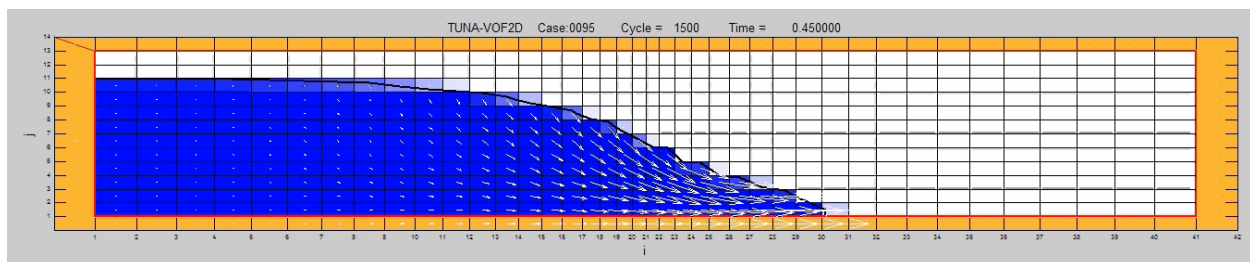


Figure-movie 7.1 Simplified surface reconstruction for the 2D dambreak problem using contour line of  $F=0.5$ .

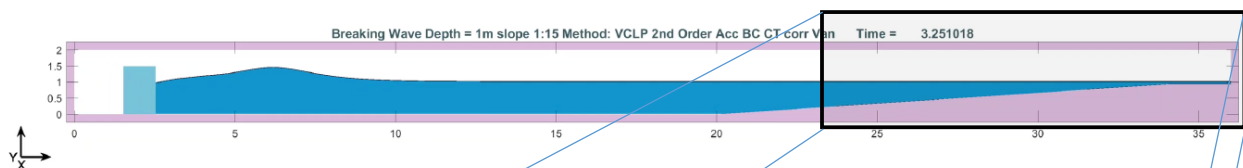
[<CLICK HERE TO WATCH MOVIE \(CASE 0095 NEW.MP4\)>](#)

## MODEL DESCRIPTION

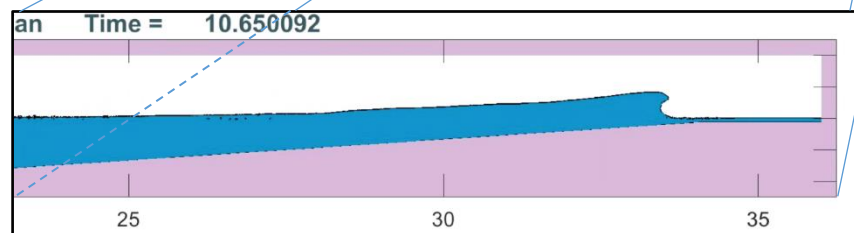
- This is a 2D wave propagating into the shore over a mild slope generating a plunging breaking wave. The time dependent Navier-Stokes model includes  $u(x,z,t)$ ,  $w(x,z,t)$  and  $F(x,z,t)$  and  $p(x,z,t)$ . Pressure is obtained by solving the Poisson equation using an iterative solver (incomplete Cholesky conjugate gradient method) of the resulting linear system of equations. Spatial step size  $\Delta x$  is 1 cm,  $\Delta z$  is 0.5 cm and time step is 0.01 s.
- Domain length is 36 m by 2 m high. The wave is generated by a piston like wavemaker to generate a soliton of 0.45 m amplitude. The water depth along the flat bottom is 1 m with a mild slope of 1:15 ramping up at the location  $x=20$  m. Here, the inclusion of the vertical direction in physics is also important for the solution of the plunging breaking wave.
- The animation depicts the wave propagation and the plunging breaking wave. Again, the free surface is defined by the F function

## MODEL SUMMARY

In this particular test, the VOF surface tracking technique proves that the solution of complex surface dynamics is possible. However, the solution requires additional computational resources for the solution of the pressure field.



[<CLICK HERE TO WATCH MOVIE \(FULLSCALE2CM.MP4\)>](#)



[<CLICK HERE TO WATCH MOVIE \(ZOOM1CM.MP4\)>](#)

EDUCATIONAL PROGRAMS  
BOOK: NUMERICAL MODELING OF TSUNAMI WAVES

CHAPTER 1

---

<UNDER CONSTRUCTION>



**CHAPTER VIII**

---

<UNDER CONSTRUCTION>

